ELSEVIER

Physica D 164 (2002) 1–27

PHYSICA D

www.elsevier.com/locate/physd

Quasi-periodically forced nonlinear Helmholtz oscillators

Arjen Doelman [a,*], A. Femius Koenderink [b], Leo R.M. Maas [c]

[a] *Korteweg-de Vries Institute, University of Amsterdam, Plantage Muidergracht 24, 1018 TV Amsterdam, The Netherlands*
[b] *Van der Waals-Zeeman Institute, University of Amsterdam, Valckenierstraat 65, 1018 XE Amsterdam, The Netherlands*
[c] *Netherlands Institute for Sea Research, P.O. Box 59, 1790 AB Texel, The Netherlands*

Received 26 September 2000; received in revised form 21 September 2001; accepted 24 January 2002
Communicated by C.K.R.T. Jones

Abstract

In this paper we study a model that describes the dynamics of the tidal elevation within an almost-enclosed short basin that is connected to a tidal sea by a narrow strait. This model has the form of a forced nonlinear Helmholtz oscillator. The forcing is prescribed by the tide at sea and has a quasi-periodic character of a special nature, since the difference between the frequencies of the lunar and solar components of the forcing tide are very small. We focus on the interactions between the nonlinearity in the oscillator caused by the geometry of the basin, and the external forcing tide. The behavior of small amplitude solutions of the weakly (and quasi-periodically) forced Helmholtz oscillator is studied by a combination of the averaging method and the Melnikov method. We construct three different Melnikov functions. These Melnikov functions enable us to distinguish between six structurally different types of chaotic behavior. © 2002 Elsevier Science B.V. All rights reserved.

Keywords: Tidal dynamics; Nonlinear oscillators; Quasi-periodic forcing; Chaotic behavior

1. Introduction

It is well-known that tidal elevations within basins such as bays, fjords and estuaries are strongly influenced by the characteristics of the basin. If there is (almost) a resonance between the exterior tide at sea and an eigen-frequency of the basin, the amplitude of the tide within the basin will be much larger than that of the exterior forcing tide. This amplification is a strictly linear phenomenon and is well understood [3,11].

However, an externally driven tidal basin is a nonlinear system. In this paper we will study some of the nonlinear aspects of externally driven tidal systems. We will focus on the impact of the characteristics of the basin on the tidal dynamics and its relation to the tide at sea.

Among the most simple physical models for a 'tidal oscillator' are those that describe the behavior of the tide within an almost-enclosed short basin that is connected to a tidal sea by a narrow strait. In such basins, the tide is generally governed by the pumping or Helmholtz (eigen-)mode, in which the water level within the basin rises and sinks in unison [11]. In [16] it was shown that the evolution of the amount of water in excess of the amount

* Corresponding author.
E-mail address: doelman@science.uva.nl (A. Doelman).

PII: S0167-2789(02)00361-5

of water present in such a basin in the absence of tides—the *excess volume* v—can be modeled by the following second-order equation:

$$\ddot{v} + \zeta(v) = \zeta_{\text{ext}}(t) - \gamma(\dot{v}). \tag{1.1}$$

Here $\zeta(v)$ and $\zeta_{\text{ext}}(t)$ denote, respectively, the surface elevation within the basin and in the exterior sea, the latter is assumed to be a given function of time. Their difference provides the pressure gradient that drives the flow u along the connecting strait ($\dot{u} \sim \zeta_{\text{ext}} - \zeta$). This flow generates changes in the excess volume ($\dot{v} \sim u$). Their combination yields (1.1), in which the term $\gamma(\dot{v})$ is added to represent friction effects. See [8,16] for more details on the derivation of this model.

There are two (potentially) nonlinear terms in this externally driven *Helmholtz oscillator*: the term $\zeta(v)$ that describes the surface elevation as a function of the (excess) volume of water within the basin, i.e. $\zeta(v)$ is determined by the *geometry* of the basin, and the friction term $\gamma(\dot{v})$ (see [28] for a derivation of a (nonlinear) expression for $\gamma(\dot{v})$). In order to be able to fully focus on the influence of the geometry of the basin on the dynamics of (1.1), we will only consider linear friction effects in this paper.

The Helmholtz frequency σ_H of a tidal basin of the above type is (in unscaled form) given by

$$\sigma_H = \sqrt{\frac{BDg}{A_0 L}}, \tag{1.2}$$

where D is the (maximum) depth of the basin, A_0 the surface area of the basin 'at rest' (i.e. $v = 0$), B and L the width and length of the strait, respectively, and g is the gravitational acceleration constant [16]. In the nonlinear system (1.1), the Helmholtz frequency σ_H is identical to the frequency associated to the center point of the linearization around $(v, \dot{v}) = (0, 0)$ of the integrable Helmholtz oscillator, i.e. (1.1) without forcing or friction terms. In that sense, σ_H is a quantity that measures linear effects, it neglects all nonlinear information on the geometry of the basin.

In this paper we extend the concept of the linear Helmholtz frequency into the nonlinear regime, by relating it to the period $\mathcal{T}_0(H)$ of the periodic orbits of the integrable nonlinear Helmholtz oscillator as a function of the energy (or Hamiltonian) H. By construction, it follows that $\sigma_H = 2\pi/\mathcal{T}_0(0)$, where $\mathcal{T}_0(0)$ is the linearized period of the center point at $H = 0$ (Section 2). The period $\mathcal{T}_0(H)$ depends strongly on the characteristics of the basin. We will show that $\mathcal{T}_0(H)$ remains bounded for all 'allowable' H and that it is in general not a monotonically increasing function, as is the case for most mechanical oscillators.

Of course, σ_H can be scaled to 1 (or $\mathcal{T}_0(0)$ to 2π). However, the unscaled σ_H varies over quite a large range in natural basins. Small-scale coastal bays and fjords typically have Helmholtz periods ranging from a few minutes up to perhaps an hour [10,14]. Sometimes the Helmholtz mode seems to prevail also in still larger-scale areas, like almost-enclosed lakes and seas [16]. This may lead to Helmholtz periods up to 24 h, as was estimated for the Gulf of Mexico [19]. Thus, by scaling σ_H to 1, and thinking of variations at sea as being principally of tidal origin, we have to allow for external forcing terms $\zeta_{\text{ext}}(t)$ in (1.1) that evolve on time scales of the same order as the integrable Helmholtz oscillator, or $\zeta_{\text{ext}}(t)$ that vary significantly slower than the Helmholtz oscillator. In this paper we will focus on the former case, the latter case has been briefly considered in [17].

The external forcing term $\zeta_{\text{ext}}(t)$ is not an exactly periodic function of time. The tide at sea consists of lunar and solar components, and may contain annual, diurnal, semi-diurnal and, as a result of nonlinearity, all kinds of harmonic combination frequencies. Frequently, the tide is dominated by just its semi-diurnal components, giving rise to the well-known (linear) fortnightly modulation (spring-neap cycle). The dominant lunar component, the semi-diurnal M_2 tide, has a frequency $\omega = 1.4056 \times 10^{-4}\,\text{s}^{-1}$, i.e. a period of $\approx$12 h 25 min; the semi-diurnal solar S_2 tide has $\omega_{\text{sol}} = 1.4544 \times 10^{-4}\,\text{s}^{-1}$: the exact 12 h period. These frequencies are, of course, almost the same: $|\omega - \omega_{\text{sol}}|/\omega = 3.47 \times 10^{-2} \ll 1$. Thus, $\zeta_{\text{ext}}(t)$ is (at least) quasi-periodic with two frequencies, ω and ω_{sol}, but the

fact that $\omega \approx \omega_{\mathrm{sol}}$ must be taken into account in an (asymptotic) analysis of (1.1), see Remark 1.1. The amplitudes of the M_2 and S_2 components can be of comparable order, although in most basins the lunar component of the tide is significantly stronger than the solar component [3].

The main goal of this paper is to develop fundamental insight in the interactions between the geometry of the basin with the external forcing tide, that is assumed to be weak (i.e. with an asymptotically small amplitude), and to unravel the mechanisms by which these interactions generate chaotic behavior in (1.1). The fact that the forced nonlinear oscillator (1.1) can exhibit chaotic solutions is, a priori, not very surprising. This was indeed already observed and studied in [17] for a certain special basin. However, the Helmholtz oscillator (1.1) distinguishes itself from most nonlinear oscillators studied in the literature, by the fact that the integrable limit only has one unique critical point, the above mentioned center point at $H = 0$ (see Section 2). Therefore, it is not possible to show that (1.1) can have chaotic solutions by directly applying the 'standard' methods as presented for instance in [9,25], since these methods are based on the assumption that the integrable planar oscillator has a homoclinic or a heteroclinic orbit. Such an orbit can of course not exist in a system without saddle points. As a consequence, we also cannot use the ideas for the analysis of weakly, quasi-periodically forced oscillators as presented in [1], and the references therein.

We can only expect non-trivial behavior in (1.1) by a resonant interaction of the weak forcing and friction terms with a periodic orbit of the integrable limit system. It is well-known [9,25] that in such cases, a purely periodic $\mathcal{O}(\varepsilon)$ forcing term can at most generate exponentially (i.e. $\mathcal{O}(\exp(-c/\varepsilon))$) thin layers of chaotic behavior. Here ε is the perturbation parameter, $0 < \varepsilon \ll 1$, that is related to the 'weakness' of the exterior forcing. We refer to [16] for such 'exponential' behavior in the Helmholtz oscillator. We thus may conclude that 'observable' chaotic behavior in (1.1) must be generated by the special character of the quasi-periodic forcing term $\zeta_{\mathrm{ext}}(t)$.

For a special basin, with a triangular structure in the vertical direction (see Section 2), it was already shown in [17], by a multiple time scale approach for small ($\mathcal{O}(\varepsilon)$) amplitude solutions in the 1:1 resonance case, that (1.1) can be transformed to a periodically driven oscillator on a time scale that is proportional to $1/|\omega - \omega_{\mathrm{sol}}|$, the time scale of the spring-neap tide cycle. In the case of a purely periodic (lunar) forcing term, this equation, called the modulation equation in [16,17], is integrable at leading order and has two homoclinic orbits to one saddle point, one, the '*inner*' orbit, inside the other, '*outer*', homoclinic orbit (under certain conditions on the parameters)—see Fig. 3. Note that this integrability agrees with, and is related to, the above mentioned fact that in this case periodic forcing can only generate chaotic behavior in regions that are thinner than ε^N for all $N > 0$. Thus, the solar component of the quasi-periodic exterior tide acts through the two time scales transformation as a periodic forcing term on this integrable system. This system can then again be considered as a weakly forced integrable system, by assuming that the amplitude of the solar component is small compared to the amplitude of the lunar component, as is the case in most basins [3]. By a standard application of the Melnikov method, it was shown in [17] that both homoclinic orbits can perturb into transversally intersecting stable and unstable manifolds to the saddle point of the associated Poincaré map, so that it is possible to show the existence of chaotic solutions to this modulation equation by the standard horseshoe map construction [9,25] (see Remark 1.1) The analysis in [17] was confirmed by the observation of chaotic behavior in numerical simulations of the modulation equation and the underlying Eq. (1.1).

In this paper we analyze the appearance of chaotic solutions in the quasi-periodically forced Helmholtz oscillator in 1:1 resonance for *general* basins. The 'modulation equation' is derived by the method of averaging (to second-order). The averaged equations are studied by Melnikov's method. The 'standard' Melnikov approach employed in [17] (for a special basin) neglects the possibility of having transversal intersections of 'mixed' type, i.e. intersections between stable and unstable manifolds that merge with distinct homoclinic orbits in the integrable limit (see also Remark 1.1). By a careful control of the 'interactions' of the Melnikov method and the method of averaging, we determine a mixed Melnikov function that measures the possibility of such intersections in the averaged system. It is found that such intersections do occur, also in regions in parameter space where neither the 'inner' nor the

'outer' homoclinic orbit can generate chaotic solutions by itself. Hence, our analysis extends the existence of chaotic behavior to regions in parameter space in which the 'standard' approach yields 'trivial' (i.e. non-chaotic) behavior (see also Remark 4.1). Moreover, we discover and classify geometrically various distinct types of complex behavior, that also cannot be detected by the 'standard' approach.

Remark 1.1. Nonlinear oscillators with quasi-periodic forcing terms with two frequencies that are 'almost' the same have also been studied in [15,26,27]. In [15] and [26] the existence of 'local' chaotic solutions, i.e. close to a center point of the integrable limit, was shown by a 'classical' analysis similar to that of [17]. As in [17], no attention has been paid in [15,26] to the possibility of 'mixed' intersections, see Remark 4.1.

2. The integrable Helmholtz oscillator

In this section we study the integrable limit associated to (1.1) for a class of general basins. We show that the flow induced by this integrable system can only have periodic 'free tidal oscillations' and a center point. We pay special attention to the period $\mathcal{T}_0(H)$ of such a free tidal oscillation as function of the 'energy' H. We determine explicit approximations for $\mathcal{T}_0(H)$ near the center point and study the behavior of $\mathcal{T}_0(H)$ in several examples.

2.1. The phase portrait

System (1.1) is integrable in the limit without friction or forcing:

$$\ddot{v} + \zeta(v) = 0. \tag{2.1}$$

The integral H of this Helmholtz oscillator is defined by

$$H = \dot{v}^2 + 2\mathcal{Z}(v), \quad \mathcal{Z}(v) = \int_0^v \zeta(\tilde{v})\,\mathrm{d}\tilde{v}. \tag{2.2}$$

The dynamics of (2.1) is determined by the *geometry* of the basin through $\zeta(v)$, the surface elevation as a function of the excess volume v. The geometry of a basin is prescribed by a 'shape function' $z = h(x, y)$: h gives a relation between z, the height or depth of the boundary or bottom of the basin and the span-wise coordinates x and y; z is normalized such that $z = 0$ refers to the mean sea level. Note that $z = 0$ also corresponds to an excess volume $v = 0$. The function $h(x, y)$ determines the so-called 'wetted area' $A(z)$ at height z: $A(z)$ is the surface area of the water in the basin at the water height z. Hence, $A(0) = A_0$ as in (1.2), the surface area of the basin at the mean sea level. The surface elevation as function of the excess volume v, the term $\zeta(v)$ in (1.1) is, of course, determined directly by the wetted area $A(z)$ (see below for the details): all geometrical 'information' of the basin enters (1.1) and (2.1) through the function $A(z)$.

In this paper we consider (scaled) two-dimensional basins given by $z = h(x)$ (see Fig. 1) or equivalently, three-dimensional basins that have a trivial, linear, structure in the y-direction. This is purely for technical reasons, since it is less cumbersome for these basins to obtain the explicit relation between the shape of the basin and the nonlinearity in (1.1) and (2.1). More realistic three-dimensional basins can be studied along the same lines: the geometry of the basin defines the nonlinear term in (1.1) and (2.1) through the relation between $h(x, y)$ and the surface area $A(z)$.

We scale the basin by assuming that $h(\pm(1/2)) = 0$ and that the basin has its maximum depth at $x = 0$: $h(0) = -1$. This implies for the Helmholtz frequency that $\sigma_H = 1$ (1.2). In order to reduce the technicalities of the calculations as much as possible, we simplify the analysis even further by assuming that $h(x)$ is symmetric

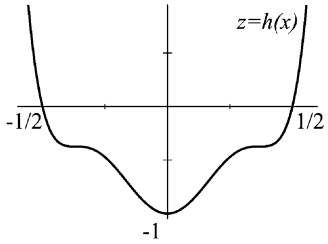

Fig. 1. A typical scaled basin of 'tidal flat type' (see Section 2.2).

($h(-x) = h(x)$), sufficiently smooth, and non-decreasing as a function of x for $x \geq 0$, see Fig. 1. As a consequence, the shape function $z = h(x)$ can be inverted for $x \geq 0$. This is of course special for the symmetric, non-decreasing functions h considered here.

Under these assumptions, the wetted area $A(z)$ of the basin at height z is given by $A(z) = 2h^{-1}(z)$ ($z \geq -1$). The excess volume $v = V(\zeta)$ is determined by its integral from the mean sea level to the surface, ζ:

$$v = V(\zeta) = \int_0^{\zeta} A(z)\,\mathrm{d}z = 2\int_0^{\zeta} h^{-1}(z)\,\mathrm{d}z. \tag{2.3}$$

The nonlinear term $\zeta(v)$ appearing in (1.1) and (2.1) can thus be expressed in terms of the geometry $h(x)$ of the basin by taking the inverse of $V(\zeta)$ in (2.3): $\zeta(v) = V^{-1}(v)$. Note that $V(\zeta)$ is monotonous and thus invertible, by construction, since $A(z) \geq 0$. As a consequence, $\zeta(v)$ also is monotonous and invertible.

In this paper we will mainly focus on the case of small amplitude oscillations, i.e. $|v| \ll 1$. In this case $\zeta(v)$ can be expanded as a Taylor series in v, with coefficients $\zeta_i = d^i\zeta/\mathrm{d}v^i(0)$, $i = 1, 2, 3, \ldots$. These coefficients can be expressed in terms of the local geometry of the basin near $z = 0$ by the above procedure:

$$\zeta_1 = 1, \qquad \zeta_2 = -\frac{2}{h_1}, \qquad \zeta_3 = 2\frac{6h_1 + h_2}{h_1^3}, \quad \ldots, \quad h_i = \frac{\mathrm{d}^i h}{\mathrm{d}x^i}\left(\frac{1}{2}\right). \tag{2.4}$$

The result $\zeta_1 = 1$ is equivalent to $\sigma_H = 1$ (1.2), it is due to our scaling of the width and depth of the basin at $z = 0$, and other, similar, scalings. Note that the geometry can be such that $h_1 = 0$. However, $h(x)$ is non-decreasing (thus $h_2 = 0$ if $h_1 = 0$), so that $\zeta(v)$ can locally still be expressed in terms of the h_i for $i = 3, 4, \ldots$, although the expansion of $\zeta(v)$ will have a different structure than in (2.4).

The monotonically increasing function $\zeta(v)$ can only be defined for $v \geq v_c^{\mathrm{low}}$ where, by (2.3),

$$v_c^{\mathrm{low}} = -2\int_{-1}^{0} h^{-1}(z)\,\mathrm{d}z = 2\int_0^{1/2} h(x)\,\mathrm{d}x < 0, \tag{2.5}$$

v_c^{low} is the (negative) excess volume of the empty basin. Thus, the solutions $\phi(t)$ of (1.1), and its integrable limit (2.1), are not allowed to enter the $\{v < v_c^{\mathrm{low}}\}$ part of the phase space by this natural condition. Since $\zeta(v)$ changes sign at $v = 0$ it follows that $\mathcal{Z}(v) > 0$ for all $v \neq 0$, which yields that $H \geq 0$ (2.2). Moreover, the monotonicity of $\zeta(v)$ also implies that the Helmholtz oscillator (2.1) only has one critical point, $(0, 0)$ at $H = 0$, of center type (2.4). Thus, the only allowed solutions of (2.1) are the one-parameter family of periodic solutions around $(0, 0)$. This family is bounded by a critical orbit $\phi_c(t)$, at the level set

$$H = H_c = 2\mathcal{Z}(v_c^{\mathrm{low}}) = 2\int_0^{1/2} h^2(x)\,\mathrm{d}x > 0 \tag{2.6}$$

(2.2) and (2.3), that is tangent to the line $\{v = v_c^{\text{low}}\}$. This orbit represents the critical oscillation in which all water has flown out of the basin at low tide. We define $v_c^{\text{high}} > 0$, and $\zeta_c^{\text{high}} > 0$, as the excess volume, and relative elevation of the water at high tide of the critical oscillation: v_c^{high} is the second zero of the equation $H = H_c = 2\mathcal{Z}(v_c^{\text{low}})$ and $\zeta_c^{\text{high}} = \zeta(v_c^{\text{high}})$. Note that the excess volume and the (relative) elevation of the water in the basin at high tide are in general not the same as the equivalent quantities at low tide, i.e. $v_c^{\text{high}} \neq |v_c^{\text{low}}|$ and $\zeta_c^{\text{high}} \neq 1$ (in general).

2.2. The period of the Helmholtz oscillator

The critical orbit $\phi_c(t)$ plays a role similar to the homoclinic orbit, or the pair of heteroclinic orbits, in classical, nonlinear oscillators, such as the Duffing equation or the mathematical pendulum, in the sense that it is the boundary of a one-parameter family of periodic orbits around the center point $(0, 0)$. However, there is an essential difference: the period of the Helmholtz oscillator does not become unbounded as H approaches H_c. The period $\mathcal{T}_0(H)$ of the orbit $\phi(t; H) = (v(t; H), \dot{v}(t; H))$ is given by

$$\mathcal{T}_0(H) = 2\int_{v^{\text{low}}(H)}^{v^{\text{high}}(H)} \frac{\mathrm{d}v}{\sqrt{H - 2\mathcal{Z}(v)}}, \tag{2.7}$$

where $v^{\text{low}}(H) < 0 < v^{\text{high}}(H)$ are the v-components of the two intersections of $\phi(t; H)$ with the $\dot{v}$-axis, i.e. $v^{\text{low}}(H)$ and $v^{\text{high}}(H)$ represent the excess volumes at low and high tide. The period $\mathcal{T}_0(H)$ is the nonlinear counterpart of the classical, linear Helmholtz period $\mathcal{T}_H = 2\pi/\sigma_H$ (1.2), where $\mathcal{T}_H = \mathcal{T}_0(0)$ by construction.

The occurrence of resonances between the forcing term $\zeta_{\text{ext}}(t)$ and the free oscillations of the Helmholtz oscillator (2.1) is of crucial importance for the dynamics of the full system (1.1). Therefore, it is necessary to study the behavior of $\mathcal{T}_0$ as a function of H. Since we mainly focus on small amplitude oscillations in this paper we first give an expansion of $\mathcal{T}_0(H)$ for $H \ll 1$:

$$\mathcal{T}_0(H) = 2\pi(1 + T_2 H + \mathcal{O}(H^{3/2})), \quad T_2 = \frac{1}{48}(5\zeta_2^2 - 3\zeta_3) = -\frac{8h_1 + 3h_2}{24h_1^3} \tag{2.8}$$

(2.3) and (2.4). There are two remarkable things about this expression: (i) the leading order correction to the linear Helmholtz period/frequency (1.2) depends both on the local slope of the basin $h_1 = h'(1/2)$ and on the local *'curvature'* $h_2 = h''(1/2)$; (ii) the sign of this correction can both be positive and negative. Note that the period increases away from the center point for standard (mechanical) nonlinear oscillators (i.e. $T_2 > 0$ in these systems). In the next section we will find that T_2 plays a crucial role in the analysis of small amplitude solutions of (1.1).

The period $\mathcal{T}_0(H)$ can be expressed explicitly in terms of the geometry of the basin $h(x)$ by the transformations in (2.3). We do not present the details of this straightforward procedure here. For the critical orbit it results in

$$\mathcal{T}_c = \mathcal{T}_0(H_c) = 2\int_0^{x_c^{\text{high}}} \frac{xh'(x)}{\sqrt{-\int_0^x \xi h(\xi)h'(\xi)\,\mathrm{d}\xi}}\,\mathrm{d}x, \tag{2.9}$$

where $x_c^{\text{high}} = h^{-1}(\zeta_c^{\text{high}})$. Note that $\mathcal{T}_c$ is always bounded and that it can be both larger or smaller than the linear Helmholtz period $\mathcal{T}_H = 2\pi$.

The behavior of $\mathcal{T}_0$ as a function of H differs, in general, essentially from that in mechanical oscillators, as we shall illustrate briefly in two examples.

For the first example we consider a class of basins that generalizes the 'triangular' basin considered in [8,16,17]: $h(x; \alpha) = (2x)^\alpha - 1$, $\alpha > 0$, for $x \geq 0$, $h(-x; \alpha) = h(x; \alpha)$: $\alpha \to \infty$ gives the rectangular *linear* basin (Fig. 2c), $\alpha = 1$ the triangular basin of [8,16,17] (Fig. 2b), and $\alpha < 1$ a 'trough' (Fig. 2a), not unlike the trench often found in

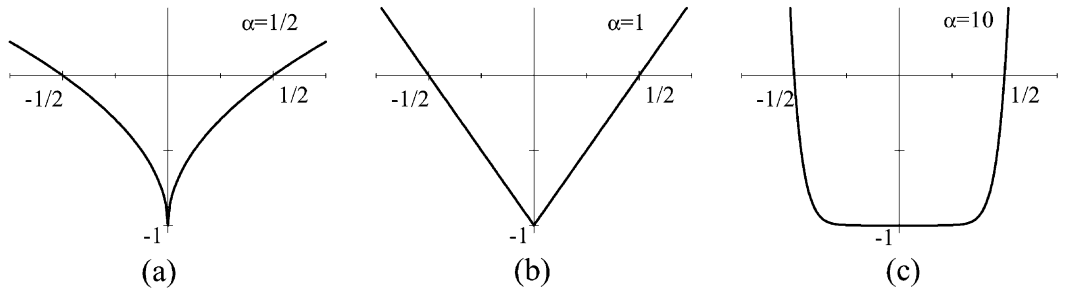

Fig. 2. Three plots of the class of basins that generalizes the 'triangular' basins studied in [8,16,17]: (a) $\alpha < 1$, a 'trough'; (b) $\alpha = 1$, the triangular basin of [8,16,17]; (c) $\alpha > 1$ a basin that limits on the rectangular basin as $\alpha \to \infty$.

tidal flat areas. It follows from (2.8) that $T_2(\alpha) = -(3\alpha + 1)/48\alpha^2 < 0$ for all $\alpha > 0$. Hence, $\mathcal{T}_0(H, \alpha)$ decreases as a function of H, for H small. By (2.9) we find (with the aid of Mathematica) that

$$\mathcal{T}_c(\alpha) = 2\sqrt{\pi}\sqrt{\frac{\alpha+1}{2\alpha}}\left(\frac{2\alpha+1}{\alpha+1}\right)^{(\alpha+1)/2\alpha}\frac{\Gamma((\alpha+1)/2\alpha)}{\Gamma((2\alpha+1)/2\alpha)},$$

where $\Gamma(z)$ is the Gamma function. It follows that $\lim_{\alpha\downarrow 0}\mathcal{T}_c(H;\alpha) = 2\sqrt{e\pi}$, $\lim_{\alpha\to\infty}\mathcal{T}_c(H;\alpha) = 2\pi$, and $\mathcal{T}_c(\alpha) \in (2\sqrt{e\pi}, 2\pi)$ (with, e.g., $\mathcal{T}_c(1) = 6$ [16,17]). Note that $\lim_{\alpha\to\infty}\mathcal{T}_0(H;\alpha) \equiv 2\pi$, since the basin becomes rectangular in this limit (Fig. 2c). Numerical approximations indicate that $\mathcal{T}_0(H;\alpha)$ decreases monotonically as a function of H.

Next, we consider models that are (loosely) inspired on the character of the tidal basins of the Wadden Sea. Large parts of these basins, the so-called tidal flats, are above sea level at low tide. This implies that the tidal oscillation in the Wadden Sea can certainly not be considered as being of small amplitude, on the contrary: in each of the tidal basins of the Wadden Sea, the ratio between the total volume of water in the basin at high tide to the (unscaled) sum $v^{\text{high}} + |v^{\text{low}}|$ ranges between 0.5 (the Marsdiep basin) to almost 1 [16].

We take $h(x;\beta) = -1 + c_1(\beta)x^2 + \beta x^4 + c_3(\beta)x^6$ with $c_{1,3}(\beta)$ such that $h((1/2);\beta) = 0$ and such that $h'(x;\beta)$ and $h''(x;\beta)$ vanish at the same points $x = \pm x_{\text{flat}}(\beta) \neq 0$. Thus, although $h(x;\beta)$ is monotonically increasing for $x \geq 0$, the basin is indeed flat at the inflection points $x = \pm x_{\text{flat}}(\beta)$ (Fig. 1). The position of the flat part of the basin, i.e. $x_{\text{flat}}(\beta)$, can be controlled by varying β: $x_{\text{flat}}(\beta) \in (0, \infty)$. With the aid of Mathematica it can be checked by the above general results on $\mathcal{T}_0(H)$ (2.8) and (2.9) that both $T_2(\beta)$ and $\mathcal{T}_0(H_c;\beta) - 2\pi$ can change sign independently within this β-family of 'tidal flat basins'. Hence, there exist basins in which $\mathcal{T}_0(H;\beta)$ can have a maximum or a minimum as a function of H for a certain $H = H_m(\beta) \in (0, H_c)$. As a consequence, the external forcing $\zeta_c(t)$ can, for instance, be in 1:1 resonance with *two* different free oscillations of the Helmholtz oscillator (2.1).

These examples show that the behavior as a function of the Hamiltonian H of the period $\mathcal{T}_0(H)$, or equivalently, the (nonlinear Helmholtz) frequency, of an integrable tidal oscillator, can be quite rich compared to the monotonic character of the period in classical examples of mechanical oscillators. As a consequence, there can also be new types of resonant interactions. This will be the subject of future research. In this paper we focus on the small amplitude case, so that $H \ll 1$.

3. Small amplitude oscillations

In this section we focus on the case of small amplitude oscillations of the excess volume $v(t)$. We scale system (1.1) such that we can apply the method of averaging and derive a generalization of the modulation equation

in [17]. The integrable limit can again have a saddle point with an 'inner' and an 'outer' homoclinic orbit. The existence of these orbits is determined completely by the relation between the characteristics (frequency, amplitude) of the dominant, lunar component of the exterior tide and the deviation of the nonlinear Helmholtz frequency from the linear Helmholtz frequency σ_H. This deviation, i.e. in essence $\mathcal{T}_0(H) - \mathcal{T}_0(0)$ for small H, is determined by the geometry of the basin. Thus, we find that the possibility of a chaotic response of the tide in a basin to a given exterior forcing tide, is determined by the geometry of that basin.

The main motivation to use the method of averaging is that it enables us to obtain full control on the validity of the approximation on the relevant time scale [22]. This is necessary, since a Melnikov analysis requires validity on long time scales. It is shown that a Melnikov analysis of the averaged system is possible, in the sense that the approximation is valid on the time scales necessary for the Melnikov method. However, it has to be assumed that the ratio of the amplitude of the solar and the lunar exterior tide is $\mathcal{O}(\delta)$ with $0 < \varepsilon \ll \delta \ll 1$. The analysis cannot be expected to be valid when $\delta = \mathcal{O}(\varepsilon)$, where ε is the asymptotic parameter of the averaging procedure, since in that case one has to be able to approximate the flow on time scales that exceed those for which the validity of the approximation is guaranteed by the averaging method.

Next, we study all possible intersections of the stable and unstable manifolds to the saddle point of the Poincaré map associated to the weakly forced modulation equation. We show that apart from the two 'standard' Melnikov functions $\mathcal{M}_{\text{in}}(T_0)$ and $\mathcal{M}_{\text{out}}(T_0)$, there is a third Melnikov function, $\mathcal{M}_{\text{mixed}}(T_0)$ that measures the distance between stable and unstable manifolds that merge with different homoclinic orbits in the limit $\delta \to 0$. All three Melnikov functions can be represented by explicit expressions. The 'mixed' Melnikov function is constructed by a careful analysis of the path of an (un)stable manifold as it follows the framework spanned by both the outer and the inner (unperturbed) homoclinic orbits. Here, the passage of a manifold near the saddle point requires special attention (see also Remark 3.5).

3.1. The averaged equations

We introduce $0 < \varepsilon \ll 1$ and $V = V(t)$ by $v = \varepsilon V$ and use (2.4) to obtain a leading order expansion of the left-hand side of (1.1) in terms of the geometry. We then 'tune' the magnitude (with respect to ε) of the quasi-periodic forcing term and of the friction term at the right-hand side of (1.1) to the character of the integrable limit (2.1) of (1.1)—see Remark 3.1. Therefore, we assume that $\zeta_{\text{ext}}(t) = \varepsilon^3 Z(t)$ and $\gamma(\dot{v}) = \varepsilon^2 C\dot{v}$, so that (1.1) can be written as

$$\ddot{V} + V = -\tfrac{1}{2}\varepsilon\zeta_2 V^2 + \varepsilon^2[-\tfrac{1}{6}\zeta_3 V^3 + Z(t) - C\dot{V}] + \mathcal{O}(\varepsilon^3). \tag{3.1}$$

Note that we thus have assumed that the surface elevation of the exterior sea $\zeta_{\text{ext}}(t) = \mathcal{O}(\varepsilon^3) \ll \zeta(v) = \zeta(\varepsilon V) = \mathcal{O}(\varepsilon)$, the surface elevation within the basin. This amplification is in essence the 'strictly linear phenomenon' due to resonance, mentioned in Section 1 [3,11]. We furthermore assume that both the semi-diurnal lunar M_2 tide and the semi-diurnal solar S_2 tide are almost in 1:1 resonance with the small amplitude periodic orbits of the integrable system (2.1). By (2.2) and (2.8) we know that $\mathcal{T}_0 - 2\pi$ is $\mathcal{O}(\varepsilon^2)$ in an $\mathcal{O}(\varepsilon)$ neighborhood of the center point. Therefore we can now introduce an explicit, simplified, expression for the external quasi-periodic forcing term:

$$Z(t) = F\,\cos(\omega t + \theta) + F_{\text{sol}}\,\cos(\omega_{\text{sol}} t + \theta_{\text{sol}}), \quad \omega = 1 + \varepsilon^2\sigma, \;\; \omega_{\text{sol}} = 1 + \varepsilon^2\sigma_{\text{sol}} \tag{3.2}$$

so that, by construction $\omega \approx \omega_{\text{sol}} \approx 1$. The weak quasi-periodicity of the forcing term is established by the condition $\sigma \neq \sigma_{\text{sol}}$. Note that we have thus assumed (for simplicity) that the external tide $\zeta_{\text{ext}}(t)$ only has semi-diurnal components (i.e. M_4, S_4, etc., and diurnal components have all been neglected).

The scaled Eq. (3.1) can be brought into a 'standard form for averaging' [9,22] by introducing the polar coordinates $R(t)$ and $\Phi(t)$ through the phase-amplitude transformation,

$$V(t) = R(t)\,\cos(\omega t - \Phi(t)), \quad \dot{V}(t) = -\omega R(t)\,\sin(\omega t - \Phi(t)), \tag{3.3}$$

so that (3.1) can be written as a three-dimensional t-periodic system

$$\begin{aligned}
\dot{R} &= \varepsilon\left[\frac{1}{2}\zeta_2 R^2\,\cos^2(\omega t-\Phi)\,\sin(\omega t-\Phi)\right]+\varepsilon^2[G(R,\Phi,\Sigma,\omega t)\,\sin(\omega t-\Phi)]+\mathcal{O}(\varepsilon^3),\\
\dot{\Phi} &= \varepsilon\left[-\frac{1}{2}\zeta_2 R\,\cos^3(\omega t-\Phi)\right]+\varepsilon^2\left[-\frac{1}{R}G(R,\Phi,\Sigma,\omega t)\,\cos(\omega t-\Phi)\right]+\mathcal{O}(\varepsilon^3),\\
\dot{\Sigma} &= \varepsilon^2[\Omega],
\end{aligned} \tag{3.4}$$

where

$$\begin{aligned}
G(R,\Phi,\Sigma,\omega t) = {}& \tfrac{1}{6}\zeta_3 R^3\,\cos^3(\omega t-\Phi)-2\sigma R\,\cos(\omega t-\Phi)-F\,\cos(\omega t+\theta),\\
& -F_{\mathrm{sol}}\,\cos(\omega t+\Sigma)-C\omega R\,\sin(\omega t-\Phi),\\
\Omega = {}& \sigma_{\mathrm{sol}}-\sigma.
\end{aligned} \tag{3.5}$$

The special quasi-periodic structure of the driving force (3.2) has been incorporated in the slow variable Σ. Note that it is immediately clear from the structure of (3.1) that first-order averaging will yield a trivial result, i.e. the 'net contribution' of the term $\varepsilon\zeta_2 V^2$ is 0, so that the averaged quantities $\bar{R}$ and $\bar{\Phi}$ are constant on a $1/\varepsilon$ time scale (at leading order) [9,22]. Therefore, we average system (3.4) to second-order [22] and obtain

$$\begin{aligned}
\bar{R}' &= -\tfrac{1}{2}C\bar{R}+\tfrac{1}{2}[F\,\sin(\bar{\Phi}+\theta)+F_{\mathrm{sol}}\,\sin(\bar{\Phi}+\bar{\Sigma})]+\mathcal{O}(\varepsilon),\\
\bar{\Phi}' &= \sigma+\frac{1}{48}(5\zeta_2^2-3\zeta_3)\bar{R}^2+\frac{1}{2\bar{R}}[F\,\cos(\bar{\Phi}+\theta)+F_{\mathrm{sol}}\,\cos(\bar{\Phi}+\bar{\Sigma})]+\mathcal{O}(\varepsilon),\\
\bar{\Sigma}' &= \Omega+\mathcal{O}(\varepsilon),
\end{aligned} \tag{3.6}$$

where the derivatives are now taken with respect to the natural slow time $T=\varepsilon^2 t$ associated to the second-order averaging procedure. Since $(\bar{R},\bar{\Phi},\bar{\Sigma})$ only evolves on the $\mathcal{O}(1/\varepsilon^2)$ time scale, i.e. since first-order averaging yields a trivial result, it follows that the approximation of (R,Φ,Σ) by $(\bar{R},\bar{\Phi},\bar{\Sigma})$ is $\mathcal{O}(\varepsilon^2)$ accurate on a $\mathcal{O}(1/\varepsilon^2)$ time scale, i.e. the solutions of (3.6) give $\mathcal{O}(\varepsilon^2)$ accurate approximations of the solutions of (3.4) as long as $T=\mathcal{O}(1)$ [22] (see Remark 3.2).

The averaged equation can be interpreted more directly in Cartesian coordinates, therefore we introduce $X(T)$ and $Y(T)$ by

$$X(T)=\bar{R}\,\cos(\bar{\Phi}),\qquad Y(T)=\bar{R}\,\sin(\bar{\Phi}), \tag{3.7}$$

so that (3.6) can be brought into the leading order two-dimensional form

$$\begin{aligned}
X' &= -Y[\sigma+T_2(X^2+Y^2)]+\tfrac{1}{2}F\,\sin\theta-\tfrac{1}{2}CX+\tfrac{1}{2}F_{\mathrm{sol}}\,\sin(\Omega T+\Sigma_0),\\
Y' &= X[\sigma+T_2(X^2+Y^2)]+\tfrac{1}{2}F\,\cos\theta-\tfrac{1}{2}CY+\tfrac{1}{2}F_{\mathrm{sol}}\,\cos(\Omega T+\Sigma_0),
\end{aligned} \tag{3.8}$$

where we have used (2.8). Note that (3.8) can also be derived more directly from (3.1) by using the van der Pol transformation [22] instead of the phase-amplitude transformation (3.3).

Observe that all 'information' on the geometry of the basin is concentrated in a single coefficient, T_2, the leading order approximation of the difference between the classical, linear Helmholtz period $\mathcal{T}_H=2\pi/\sigma_H$ and its nonlinear generalization $\mathcal{T}_0(H)$ (2.7) and (2.8). We can indeed conclude that the nonlinear Helmholtz period (or frequency) is the dominant quantity in the representation of the structure of a basin in the description of its tidal dynamics, like in the classical, linear case [11,28]. Since we are interested in the influence of the geometry of the basin on the dynamics of (1.1) we assume that $T_2\neq 0$, although it should be noted that T_2 can be 0 with a non-trivial geometry (2.8).

Without loss of generality, we set $\theta = 0$; θ originally described a phase shift in (3.2), changing θ corresponds through (3.3) and (3.7) with a rotation of X and Y in (3.8), and a shift in Σ_0.

Remark 3.1. We have made several choices to arrive at (3.1) and (3.2). Of course, the assumption that the system is in 1:1 resonance is arbitrary, different resonances can be studied along the same lines (see Section 5). The assumption that the excess volume v is small with respect to the total volume of the basin is very natural, although it is certainly not valid for all natural basins, see Section 2. However, the assumptions on the relations between the magnitudes of $|v|$, $|\zeta_{\text{ext}}(t)|$, $|\gamma(\dot{v})|$ and $|\omega - \omega_{\text{sol}}|$ are motivated by the (mathematical) preference to balance the influences of all four competing components in (3.1)—the geometry, the forcing and its quasi-periodicity, and the friction. In that sense the above scalings can be interpreted as a 'significant degeneration' in the terminology of (singular) perturbation theory [5].

Remark 3.2. The 'modulation equation' (3.6) can also be obtained by the method of multiple time scales, as was done for a special 'triangular' basin (see Section 2) in [17]. Here, we prefer the method of averaging, since we need the (classical) results on the accuracy and the validity of the approximation procedure (that can for instance be found in [22]) in order to be able to apply Melnikovs method to (3.6) and (3.8).

3.2. The periodically forced Helmholtz oscillator

By setting $F_{\text{sol}} = 0$, we recover the case of a periodic, lunar, forcing in (1.1), see (3.2). System (3.8) can now be seen as a Hamiltonian system with friction. This system has been studied in more detail in [16,17] in the special case of a 'triangular' domain, so that $T_2 = -(1/2)$ (see Section 2). The integrable structure is common for weakly, periodically forced planar systems at resonance: in weakly forced systems, non-trivial, chaotic, behavior can only be expected near saddle connections, see for instance [9,25].

The integrable limit is obtained by setting, in addition, $C = 0$. The Hamiltonian reads

$$\mathcal{H}(X, Y) = -\frac{1}{4T_2}[\sigma + T_2(X^2 + Y^2)]^2 - \frac{1}{2}FX. \tag{3.9}$$

The critical points of the Hamiltonian system are given by

$$T_2X^3 + \sigma X + \tfrac{1}{2}F = 0, \qquad Y = 0. \tag{3.10}$$

Hence, if $\text{sign}(T_2) = \text{sign}(\sigma)$, then there is only one critical point (of center type) in the integrable limit, if $\text{sign}(T_2) \neq \text{sign}(\sigma)$, then there are up to three critical points (by varying F): two centers and one saddle (see Fig. 3). Note

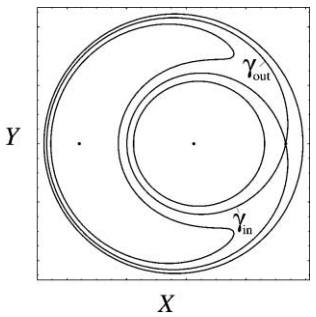

Fig. 3. The unperturbed, i.e. integrable, averaged system: (3.8) with $C = F_{\text{sol}} = 0$; F is chosen such that there are two center points, a saddle point $P_{\text{s}} = (X_{\text{s}}, 0)$, and two homoclinic orbits to the saddle P_{s}, the outer orbit $\gamma_{\text{out}}^{\text{hom}}$ and the inner orbit $\gamma_{\text{in}}^{\text{hom}}$.

that only the latter, most interesting, case corresponds to a situation in which the frequency of the dominant (lunar) tide, $\omega = 1 + \varepsilon^2\sigma$, (3.2) can be in exact 1:1 resonance with one of the natural small amplitude oscillations of the basin with $H = \varepsilon^2\hat{H}$ (2.1) and (2.2), since the nonlinear Helmholtz frequency of such an oscillation is given by $\sigma_H(\varepsilon^2\hat{H}) = 2\pi/\mathcal{T}_0(\varepsilon^2\hat{H}) = 1 - \varepsilon^2\hat{H}T_2 + \mathcal{O}(\varepsilon^3)$ (2.8).

In the next (sub)sections we will consider (3.8) as a periodically forced integrable system. We will assume that both C and F_{sol} are asymptotically small, of $\mathcal{O}(\delta)$, with $0 < \varepsilon \ll \delta \ll 1$ (see Section 3.3 for a detailed motivation). Since one of the main themes of this paper is to show that a weakly, quasi-periodically forced Helmholtz oscillator exhibits chaotic behavior, while there are no saddle connections in the integrable limit (2.1), we will only consider the case in which there can be saddle points, and thus homoclinic orbits, in the integrable limit of the averaged system (3.8), see Remark 3.3. Hence, we can conclude that there can only be non-trivial behavior in (3.8) (with C, $F_{\mathrm{sol}} = \mathcal{O}(\delta)$), when the dominant (lunar) component of the external quasi-periodic forcing term (3.2) can be in exact resonance with one of the 'nonlinear' small amplitude periodic orbits of (2.1). Note that the geometry of the basin thus completely determines, through T_2 (2.8), the possibility of chaotic behavior, since the frequency of the lunar tide must be considered as given.

In this paper we consider $T_2 < 0 < \sigma$. The situation $\sigma < 0 < T_2$ can be transformed into this case. Without loss of generality we can set $T_2 = -1$ and $\sigma = 1$ in (3.8), by rescaling X, Y, F, C, F_{sol}. This is in essence the case studied in [17]. It follows from (3.10) that the Hamiltonian limit of (3.8), i.e. $C = F_{\mathrm{sol}} = 0$ with $\sigma = -T_2 = 1$, can only have saddle points when $-(4/9)\sqrt{3} \le F \le (4/9)\sqrt{3}$. When $F \neq 0, \pm(4/9)\sqrt{3}$ there is one saddle point, $P_{\mathrm{s}} = (X_{\mathrm{s}}, 0)$, and two critical points of center type. This saddle point defines the level set $\mathcal{H}(X, Y) = \mathcal{H}^{\mathrm{hom}}$ (3.9). There are two homoclinic orbits in this level set: an *outer* orbit $\gamma_{\mathrm{out}}^{\mathrm{hom}}(T)$ and an *inner* orbit $\gamma_{\mathrm{in}}^{\mathrm{hom}}(T)$ (see Fig. 3), both limiting on $(X_{\mathrm{s}}, 0)$. As $F \to (4/9)\sqrt{3}$, or $-(4/9)\sqrt{3}$, the saddle point merges with one of the center points; $\gamma_{\mathrm{out}}^{\mathrm{hom}}(T)$ and $\gamma_{\mathrm{in}}^{\mathrm{hom}}(T)$ merge as $F \to 0$. The X-coordinate X_{s} of P_{s} is positive for $-(4/9)\sqrt{3} < F < 0$; the case of a saddle point with a negative X-coordinate can be obtained from this by transforming $X \to -X$, $Y \to -Y$ and $F \to -F$ (which corresponds, once again, to a phase shift in (3.6)). Therefore, we focus on the case $-(4/9)\sqrt{3} < F < 0$.

In the next section we will study the influence of small, $\mathcal{O}(\delta)$, perturbation terms in the integrable limit system by the Melnikov method [9,25]. In order to perform the necessary calculations, we need explicit expressions for $\gamma_{\mathrm{out}}^{\mathrm{hom}}(T)$ and $\gamma_{\mathrm{in}}^{\mathrm{hom}}(T)$. These expressions can be obtained by introducing the auxiliary variable $S = S(T) = (X^2 + Y^2) - 1$. In terms of this new variable, the homoclinic orbits $\gamma_{\mathrm{out,in}}^{\mathrm{hom}}(T)$ correspond to $S_{\mathrm{out,in}}^{\mathrm{hom}}(T)$. It is shown in Appendix A that

$$
\begin{aligned}
S_{\mathrm{out}}^{\mathrm{hom}}(T) &= S_{\mathrm{s}} + \left(\frac{\cosh^2 \mu T}{S_+ - S_{\mathrm{s}}} - \frac{\sinh^2 \mu T}{S_- - S_{\mathrm{s}}} \right)^{-1} = S_{\mathrm{s}} + \frac{A_{\mathrm{s}}}{-a_{\mathrm{s}} + \cosh 2\mu T}, \\
S_{\mathrm{in}}^{\mathrm{hom}}(T) &= S_{\mathrm{s}} + \left(\frac{\cosh^2 \mu T}{S_- - S_{\mathrm{s}}} - \frac{\sinh^2 \mu T}{S_+ - S_{\mathrm{s}}} \right)^{-1} = S_{\mathrm{s}} + \frac{-A_{\mathrm{s}}}{a_{\mathrm{s}} + \cosh 2\mu T}.
\end{aligned} \tag{3.11}
$$

We refer to (A.3) and (A.4) in Appendix A for explicit expressions for the constants $S_{\mathrm{s}} < 0$, $S_+ > S_{\mathrm{s}}$, $S_- < S_{\mathrm{s}}$, $A_{\mathrm{s}} > 0$, $a_{\mathrm{s}} \in (0, 1)$ and $\mu > 0$. The Melnikov analysis of the next section will be based on (3.11).

Remark 3.3. The dynamics of (3.8) in the case $\mathrm{sign}(T_2) = \mathrm{sign}(\sigma)$ and C, $F_{\mathrm{sol}} = \mathcal{O}(\delta)$ is, of course, not completely trivial. The driving frequency Ω can be in resonance with one or more periodic orbits of the integrable limit, so that one, once again, can study the system by averaging, or by the subharmonic Melnikov method [9,25] (note that these procedures are only valid for $0 < \varepsilon \ll \delta \ll 1$, see Section 3.3). Hence, one can establish the existence of various types of periodic orbits in (3.8).

3.3. Perturbed homoclinic orbits: the Melnikov functions $\mathcal{M}_{\text{out}}$ and $\mathcal{M}_{\text{in}}$

In this section and the next section we study a weakly forced version of (3.8)

$$\begin{aligned} X' &= -Y[1-(X^2+Y^2)] + \delta[-\tfrac{1}{2}\tilde{C}X - \tfrac{1}{2}F\,\cos(\Omega T)] + \mathcal{O}(\varepsilon),\\ Y' &= X[1-(X^2+Y^2)] + \tfrac{1}{2}F + \delta[-\tfrac{1}{2}\tilde{C}Y + \tfrac{1}{2}F\,\sin(\Omega T)] + \mathcal{O}(\varepsilon), \end{aligned} \tag{3.12}$$

where $\varepsilon \ll \delta \ll 1$ has been defined by the natural assumption that the amplitude of the solar tide is (asymptotically) small compared to that of the lunar tide: $F_{\text{sol}} = \delta F$ (3.2). Moreover, we have chosen $\Sigma_0 = -\pi/2$, in order to be able to compare the outcome of the Melnikov calculations with those in [17]. This choice is not at all essential: Σ_0 does not have any (leading order) influence on the existence of transversal intersections of the homoclinic orbits of (3.12) with general Σ_0 (it does have influence on the location of these intersections, but that is not relevant for the existence of Smale horseshoes, etc., see also Remark 3.6). Furthermore, we have set $\sigma = -T_2 = 1$, $\theta = 0$, as was explained in the previous section, and $C = \delta\tilde{C}$ (the tilde will be dropped in the subsequent analysis). System (3.12) can be written in the standard, autonomous form

$$\frac{\mathrm{d}}{\mathrm{d}T}\begin{pmatrix} X\\ Y\\ \Theta\end{pmatrix} = \begin{pmatrix} \dfrac{\partial \mathcal{H}}{\partial Y}(X,Y)\\ -\dfrac{\partial \mathcal{H}}{\partial X}(X,Y)\\ \Omega\end{pmatrix} + \delta\begin{pmatrix} \mathcal{G}_1(X,Y,\Theta)\\ \mathcal{G}_2(X,Y,\Theta)\\ 0\end{pmatrix} + \mathcal{O}(\varepsilon) \quad \text{for } (X,Y,\Theta)\in \mathbf{R}^2\times S^1, \tag{3.13}$$

where $\mathcal{H}(X,Y;F)$ is the Hamiltonian (3.9) and $(\mathcal{G}_1,\mathcal{G}_2)$ the $2\pi/\Omega$ periodic perturbation term. System (3.13) has a hyperbolic $2\pi/\Omega$ periodic orbit that is $\mathcal{O}(\delta)$ close to the saddle point P_{s} of the unperturbed problem. A more precise formulation of this result can be given in terms of the Poincaré map $\mathcal{P}^{T_0}$ associated to (3.13), where $T_0 \in [0, 2\pi/\Omega)$ defines the section $\Sigma^{T_0} = \{\Theta = T_0\}$ on which $\mathcal{P}^{T_0}$ is defined. There exists a neighborhood $D_{\mathcal{P}}$ of P_{s} in which the map $\mathcal{P}^{T_0}$ has a saddle point $P_\delta^{T_0}$ that is $\mathcal{O}(\delta)$ close to the saddle point P_{s} of the unperturbed ($\delta = \varepsilon = 0$) limit of (3.13). Moreover, the (local) stable and unstable manifolds of $P_\delta^{T_0}$ in $D_{\mathcal{P}}$, $W^{\text{s,u}}_{\text{loc}}(P_\delta^{T_0})$, are $\mathcal{O}(\delta)$ close to the (local) stable and unstable manifolds of P_{s} in the Hamiltonian limit system [9,25].

In the analysis of (3.13), it is essential to assume that $0 < \varepsilon \ll \delta \ll 1$, i.e. that δ is an $\mathcal{O}(1)$ quantity compared to ε. This is because the averaging method only gives $\mathcal{O}(1)$ accuracy on $\mathcal{O}(1)$ T-time intervals in (3.8) and thus in (3.13) [22]. A priori, one might think that it is thus not at all possible to apply Melnikovs method to measure the splitting distances in the perturbed homoclinic orbits of the averaged system (3.13), since this method involves integrals over (semi-)infinite time intervals. However, inside the above defined neighborhood $D_{\mathcal{P}}$ the behavior of the integrable limit persists, and one has full control over the flow generated by (3.13). There exist similar persistence results in the literature on the averaging method (see for instance [22]) that relate a critical point of the averaged system to a periodic orbit of the full system. The application of these results to the periodically forced system (3.4) without dissipation, i.e. $F_{\text{sol}} = C = 0$ in (3.4), yields that the saddle point P_{s} of the integrable system, and its local characteristics, corresponds to a periodic orbit of the original system (3.4) with the corresponding local character (note that (3.4) reduces to a two-dimensional system when there is no solar component in the forcing term, i.e. when $F_{\text{sol}} = \delta F = 0$, see (3.5)). The combination of the two persistence results yields that one only needs to approximate the global stable and unstable manifolds of $P_\delta^{T_0}$, $W^{\text{s,u}}(P_\delta^{T_0})$, outside $D_{\mathcal{P}}$, and $W^{\text{s,u}}(P_\delta^{T_0})$ only spend a finite time interval outside $D_{\mathcal{P}}$ in the application of the Melnikov method [9,25]. Assuming that the magnitude δ of the perturbations in (3.13) is $\mathcal{O}(1)$ with respect to ε, implies that the time interval over which one needs to approximate the $W^{\text{s,u}}(P_\delta^{T_0})$ is also $\mathcal{O}(1)$ with respect to ε. Hence, when $0 < \varepsilon \ll \delta \ll 1$ there is no conflict between the application of the Melnikov method and the averaging method (see Remark 3.4).

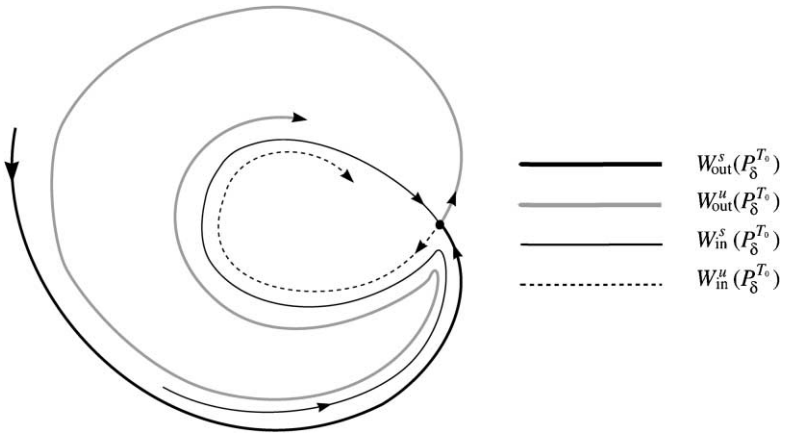

Fig. 4. A sketch of the four stable and unstable manifolds $W^{\rm s}_{\rm out}(P_\delta^{T_0})$, $W^{\rm u}_{\rm out}(P_\delta^{T_0})$, $W^{\rm s}_{\rm in}(P_\delta^{T_0})$, and $W^{\rm u}_{\rm in}(P_\delta^{T_0})$ to the saddle point $P_\delta^{T_0}$ of the Poincaré map $\mathcal{P}^{T_0}$ associated to (3.12). Note that there are no intersections in this case.

The perturbations in (3.13) will, in general, break both homoclinic orbits of $P_{\rm s}$ in the Hamiltonian limit. The Melnikov method measures the (leading order) splitting distance between the stable and unstable manifolds of $P_\delta^{T_0}$, $W^{\rm s}(P_\delta^{T_0})$ and $W^{\rm u}(P_\delta^{T_0})$. In standard applications of the Melnikov method [9,25] there is only one homoclinic orbit to the saddle point in the integrable limit, so that one only has to measure the distance between those branches of the stable and unstable manifolds that correspond to that one homoclinic orbit. The system studied in this paper (3.13) has two homoclinic orbits to the same saddle point in the integrable limit, $\gamma^{\rm hom}_{\rm out}(T)$ and $\gamma^{\rm hom}_{\rm in}(T)$ (Section 3.2). Thus, we have to distinguish between two pairs of stable and unstable manifolds, $W^{\rm s,u}_{\rm out}(P_\delta^{T_0})$ and $W^{\rm s,u}_{\rm in}(P_\delta^{T_0})$ (see Fig. 4).

In this section we will determine explicit expressions for the 'standard' Melnikov functions $\mathcal{M}_{\rm out}(T_0)$ and $\mathcal{M}_{\rm in}(T_0)$; $\mathcal{M}_{\rm out}(T_0)$ measures the splitting distance between $W^{\rm s}_{\rm out}(P_\delta^{T_0})$ and $W^{\rm u}_{\rm out}(P_\delta^{T_0})$, $\mathcal{M}_{\rm in}(T_0)$ between $W^{\rm s}_{\rm in}(P_\delta^{T_0})$ and $W^{\rm u}_{\rm in}(P_\delta^{T_0})$. This distance is measured at a reference point $\gamma^{\rm hom}_{\rm out,in}(0)$ in terms of the natural weighted distance associated to the Hamiltonian $\mathcal{H}$ of the integrable limit (3.9) [9,25]. Note that one has to multiply $\mathcal{M}_{\rm out,in}(T_0)$ with $\delta/\|(\partial\mathcal{H}/\partial X(\gamma^{\rm hom}_{\rm out,in}(0)), \partial\mathcal{H}/\partial Y(\gamma^{\rm hom}_{\rm out,in}(0)))\|$ to obtain the expression for the (leading order) Euclidian distance between $W^{\rm s}_{\rm out,in}(P_\delta^{T_0})$ and $W^{\rm u}_{\rm out,in}(P_\delta^{T_0})$ at the point $\gamma^{\rm hom}_{\rm out,in}(0)$ in a cross-section that is perpendicular to the unperturbed homoclinic manifold [9,25]. We will always refer to this weighted 'energy' distance function when we measure the distance between two manifolds.

In the next section we will consider the 'mixed' intersections, $W^{\rm u}_{\rm out}(P_\delta^{T_0}) \cap W^{\rm s}_{\rm in}(P_\delta^{T_0})$ and $W^{\rm s}_{\rm out}(P_\delta^{T_0}) \cap W^{\rm u}_{\rm in}(P_\delta^{T_0})$.

It follows from the standard theory [9,25] that

$$\mathcal{M}_{\rm out,in}(T_0) = \int_{-\infty}^{\infty} \left[\begin{pmatrix} \dfrac{\partial \mathcal{H}}{\partial X}(\gamma_0(T-T_0)) \\ \dfrac{\partial \mathcal{H}}{\partial Y}(\gamma_0(T-T_0)) \end{pmatrix} \cdot \begin{pmatrix} \mathcal{G}_1(\gamma_0(T-T_0), \Omega T) \\ \mathcal{G}_2(\gamma_0(T-T_0), \Omega T) \end{pmatrix} \right] {\rm d}T, \tag{3.14}$$

where $\gamma_0(T) = (X_0(T), Y_0(T)) = \gamma^{\rm hom}_{\rm out,in}(T)$ (Section 3.2). The Melnikov functions $\mathcal{M}_{\rm out,in}(T_0)$ can be computed explicitly using the results of the previous section and Appendix A. It is shown in Appendix B that

$$\begin{aligned} \mathcal{M}_{\rm out}(T_0; \Omega, C, F) &= -2\left[C\left(\phi_{\rm out} - \frac{3\tan\phi_{\rm out}}{3+\tan^2\phi_{\rm out}} \right) + \frac{\pi\Omega^2}{\sinh k_{\rm s}\pi} {\rm e}^{k_{\rm s}\phi_{\rm out}} \cos(\Omega T_0) \right], \\ \mathcal{M}_{\rm in}(T_0; \Omega, C, F) &= -2\left[C\left(-\phi_{\rm in} + \frac{3\tan\phi_{\rm in}}{3+\tan^2\phi_{\rm in}} \right) + \frac{\pi\Omega^2}{\sinh k_{\rm s}\pi} {\rm e}^{-k_{\rm s}\phi_{\rm in}} \cos(\Omega T_0) \right], \end{aligned} \tag{3.15}$$

where $k_s = \Omega/\mu$, $\phi_{out,in}$ are determined by

$$\cos\phi_{out} = -a_s \text{ with } \phi_{out} \in \left(\frac{\pi}{2}, \pi\right), \quad \cos\phi_{in} = a_s \text{ with } \phi_{in} = \pi - \phi_{out} \in \left(0, \frac{\pi}{2}\right), \tag{3.16}$$

and μ and a_s are given in (A.4). We note that a simple zero of $\mathcal{M}_{out}(T_0)$, respectively $\mathcal{M}_{in}(T_0)$, corresponds to a transversal intersection of $W^s_{out}(P_\delta^{T_0})$ and $W^u_{out}(P_\delta^{T_0})$, respectively $W^s_{in}(P_\delta^{T_0})$ and $W^u_{in}(P_\delta^{T_0})$ [9,25].

Remark 3.4. The 'interactions' of the Melnikov method and the averaging method have been discussed in more detail in [9]. The limitations on the accuracy and the time scales of the approximation by an averaged system also imply that the leading order correction terms in an averaged system like (3.13), that can be computed by another round of averaging, cannot be used as additional 'input' in a Melnikov calculation, although such input might lead to interesting, but in general spurious, phenomena in quasi-periodically forced oscillators [27].

3.4. The 'mixed' Melnikov function $\mathcal{M}_{mixed}$

Due to the presence of two homoclinic orbits emanating from the same saddle point P_s in the integrable limit, there can also be intersections of the outer stable or unstable manifolds of the saddle point $P_\delta^{T_0}$, $W^{s,u}_{out}(P_\delta^{T_0})$ of the Poincaré map $\mathcal{P}^{T_0}$ associated to (3.13) with the inner unstable or stable manifolds of $P_\delta^{T_0}$, $W^{u,s}_{in}(P_\delta^{T_0})$ (see Figs. 4 and 7).

In this section we will construct a 'mixed' Melnikov function $\mathcal{M}_{mixed}(T_0)$ that measures the distance between the manifolds $W^u_{out}(P_\delta^{T_0})$ and $W^s_{in}(P_\delta^{T_0})$. We refer to Remark 3.5 for some background to the ideas presented in this section.

First, we need to assume that either $\mathcal{M}_{out}(T_0) \neq 0$ for all T_0, so that $W^u_{out}(P_\delta^{T_0}) \cap W^s_{out}(P_\delta^{T_0}) = \emptyset$, or that $\mathcal{M}_{in}(T_0) \neq 0$ for all T_0, i.e. $W^s_{in}(P_\delta^{T_0}) \cap W^u_{in}(P_\delta^{T_0}) = \emptyset$. If neither of these conditions hold, then both pairs, $W^{s,u}_{out}(P_\delta^{T_0})$ and $W^{s,u}_{in}(P_\delta^{T_0})$, intersect countably many times near $P_\delta^{T_0}$ and both generate the well-known homoclinic tangle structure [9,25], see Fig. 7d. In Section 4.2 we shall show that countably many 'lobes' ([25] and Remark 4.2) of both $W^u_{out}(P_\delta^{T_0})$ and $W^s_{in}(P_\delta^{T_0})$ will intersect any (transversal) cross-section at any reference point on the orbits of either γ^{hom}_{out} or γ^{hom}_{in} (see Fig. 7d). Hence, trying to measure the distance between $W^u_{out}(P_\delta^{T_0})$ and $W^s_{in}(P_\delta^{T_0})$ is in a sense irrelevant in the case that both $\mathcal{M}_{out}(T_0)$ and $\mathcal{M}_{in}(T_0)$ have zeroes.

The outer Melnikov function $\mathcal{M}_{out}(T_0)$ cannot be positive for all T_0, since the non-oscillating component of $\mathcal{M}_{out}$ (i.e. the component that does not depend on T_0) is always negative ((3.15), recall that $\phi_{out} \in (\pi/2, \pi)$ (3.16)). Thus, the condition $\mathcal{M}_{out}(T_0) \neq 0$ for all T_0 implies $\mathcal{M}_{out}(T_0) < 0$ for all T_0. A similar argument shows that $\mathcal{M}_{in}(T_0)$ must be positive when it is assumed that $\mathcal{M}_{in}(T_0) \neq 0$ for all T_0. Note that these conclusions are in essence equivalent to the observation that both center points of the integrable limit system of (3.12), i.e. $\delta = \varepsilon = 0$ in (3.12), become attractors when one introduces friction to the system (but no periodic forcing), see [16].

The result on the sign of $\mathcal{M}_{out}(T_0)$ also implies that the outer stable manifold $W^s_{out}(P_\delta^{T_0})$ will be 'outside' the unstable outer manifold $W^u_{out}(P_\delta^{T_0})$ when $\mathcal{M}_{out}(T_0) \neq 0$ for all T_0 (see Figs. 4 and 7a). Hence, $W^s_{out}(P_\delta^{T_0})$ will spiral outwards, so that the possibility of having intersections of $W^s_{out}(P_\delta^{T_0})$ with $W^u_{in}(P_\delta^{T_0})$ is excluded. By the sign of $\mathcal{M}_{in}(T_0)$ we know that the unstable inner manifold $W^u_{in}(P_\delta^{T_0})$ will be 'inside' $W^s_{in}(P_\delta^{T_0})$ when we assume that $\mathcal{M}_{in}(T_0) \neq 0$ for all T_0 (Figs. 4 and 7a). Hence, $W^u_{in}(P_\delta^{T_0})$ will spiral inwards, so that there can again be no intersections of $W^s_{out}(P_\delta^{T_0})$ with $W^u_{in}(P_\delta^{T_0})$.

We conclude that the only 'measurable' mixed intersections can occur between $W^u_{out}(P_\delta^{T_0})$ and $W^s_{in}(P_\delta^{T_0})$. Note that this does not imply that $W^s_{out}(P_\delta^{T_0}) \cap W^u_{in}(P_\delta^{T_0}) = \emptyset$ for all parameter combinations: $W^s_{out}(P_\delta^{T_0})$ and

$W^{\mathrm{u}}_{\mathrm{in}}(P_\delta^{T_0})$ will intersect when both $\mathcal{M}_{\mathrm{out}}(T_0)$ and $\mathcal{M}_{\mathrm{in}}(T_0)$ have zeroes (the 'double chaos' case, see Section 4 and Fig. 7d).

We now assume that $\mathcal{M}_{\mathrm{out}}(T_0) \neq 0$ for all T_0, so that $W^{\mathrm{u}}_{\mathrm{out}}(P_\delta^{T_0}) \cap W^{\mathrm{s}}_{\mathrm{out}}(P_\delta^{T_0}) = \emptyset$. The outer unstable manifold $W^{\mathrm{u}}_{\mathrm{out}}(P_\delta^{T_0})$ will thus return to the (small) neighborhood $D_\mathcal{P}$ of P_{s} and $P_\delta^{T_0}$. By taking the reference point $\gamma^{\mathrm{hom}}_{\mathrm{out}}(0)$ at the boundary of $D_\mathcal{P}$, we may conclude that the (leading order) distance between $W^{\mathrm{u}}_{\mathrm{out}}(P_\delta^{T_0})$ and $W^{\mathrm{s}}_{\mathrm{loc,out}}(P_\delta^{T_0})$ (the local outer stable manifold of $P_\delta^{T_0}$) at the 'entrance point' $Q^D_{\mathrm{entr}} \in \partial D_\mathcal{P}$ is given by $\mathcal{M}_{\mathrm{out}}(T_0)$. In order to determine a distance between $W^{\mathrm{u}}_{\mathrm{out}}(P_\delta^{T_0})$ and $W^{\mathrm{s}}_{\mathrm{in}}(P_\delta^{T_0})$ we must first follow $W^{\mathrm{u}}_{\mathrm{out}}(P_\delta^{T_0})$ during its passage near $P_\delta^{T_0}$ (see Remark 3.5).

It follows from the construction of $\mathcal{M}_{\mathrm{out}}(T_0)$ [9,25] that this conclusion is only valid when we assume that $\partial D_\mathcal{P}$ coincides, at the intersection, with a (large enough) piece of the line through the intersection point, normal to the outer homoclinic manifold of the integrable limit system (i.e. the orbit of $\gamma^{\mathrm{hom}}_{\mathrm{out}}(T)$). Therefore, we will assume from now on that the neighborhood $D_\mathcal{P}$ of $P_\delta^{T_0}$ has the shape of a quadrangle with sides perpendicular to the orbits $\gamma^{\mathrm{hom}}_{\mathrm{out,in}}$ at the four intersection points $\gamma^{\mathrm{hom}}_{\mathrm{out,in}} \cap \partial D_\mathcal{P}$. This is of course no restriction. Moreover, we choose $D_\mathcal{P}$ such that the Euclidian distance between those intersection points and the 'center' P_{s}, or equivalently $P_\delta^{T_0}$, of $D_\mathcal{P}$ is of $\mathcal{O}(\delta^k)$ for some $0 < k < 1/2$ (this is, again, no restriction [9,25]). The bounds on k will be explained (and used) in the forthcoming analysis.

Since the 'full' Eq. (3.13) is (by definition) dominated by the linear flow inside the region $D_\mathcal{P} \times S^1$, it is possible to compute the orbits of the Poincaré map $\mathcal{P}^{T_0}$ through $D_\mathcal{P}$ explicitly (to leading order), and thus to determine the path of the manifold $W^{\mathrm{u}}_{\mathrm{out}}(P_\delta^{T_0})$ through $D_\mathcal{P}$. It follows from the conditions on the 'size' of $D_\mathcal{P}$, i.e. $k > 0$, that an orbit of the map $\mathcal{P}^{T_0}$ through the entrance point Q^D_{entr} exits $D_\mathcal{P}$ after $N = \mathcal{O}(|\log\delta|)$ iterations (which is $\mathcal{O}(1)$ with respect to ε). It can be assumed (by adapting $D_\mathcal{P}$), without loss of generality, that $(\mathcal{P}^{T_0})^N(Q^D_{\mathrm{entr}}) = Q^D_{\mathrm{exit}} \in \partial D_\mathcal{P}$. Note that, in terms of the flow governed by (3.13), this corresponds to the assumption that the orbit through the point $(Q^D_{\mathrm{entr}}, 0) \in \mathbf{R}^2 \times S^1$ leaves the region $D_\mathcal{P} \times S^1$ with an 'exit' phase equal to the 'entrance' phase, i.e. that $\Theta_{\mathrm{exit}} = \Omega T_{\mathrm{exit}} = 0 \pmod{2\pi}$, where T_{exit} is the $\mathcal{O}(|\log\delta|)$ 'passage time' of that orbit through $D_\mathcal{P} \times S^1$. Since $W^{\mathrm{u}}_{\mathrm{out}}(P_\delta^{T_0}) \cap W^{\mathrm{s}}_{\mathrm{out}}(P_\delta^{T_0}) = \emptyset$ 'before' $W^{\mathrm{u}}_{\mathrm{out}}(P_\delta^{T_0})$ reached $D_\mathcal{P}$, it follows that $W^{\mathrm{u}}_{\mathrm{out}}(P_\delta^{T_0})$ does not intersect the span $\{W^{\mathrm{s}}_{\mathrm{loc,out}}(P_\delta^{T_0}) \cup W^{\mathrm{u}}_{\mathrm{loc,out}}(P_\delta^{T_0}) \cup W^{\mathrm{s}}_{\mathrm{loc,in}}(P_\delta^{T_0}) \cup W^{\mathrm{u}}_{\mathrm{loc,in}}(P_\delta^{T_0})\} \cap D_\mathcal{P}$. The *Euclidian* distance between $W^{\mathrm{u}}_{\mathrm{out}}(P_\delta^{T_0})$ and this span varies between $\mathcal{O}(\delta)$ and $\mathcal{O}(\sqrt{\delta})$ inside $D_\mathcal{P}$, due to the saddle character of $P_\delta^{T_0}$. This explains the above lower bound on the size of $D_\mathcal{P}$ ($k < 1/2$). A Taylor expansion around $P_{\mathrm{s}} = (X_{\mathrm{s}}, 0)$ yields that

$$\dot{\mathcal{H}}(X(T), Y(T), \Theta(T)) = \delta \left[\begin{pmatrix} \dfrac{\partial \mathcal{H}}{\partial X}(X(T), Y(T)) \\ \dfrac{\partial \mathcal{H}}{\partial Y}(X(T), Y(T)) \end{pmatrix} \cdot \begin{pmatrix} \mathcal{G}_1(X(T), Y(T), \Theta(T)) \\ \mathcal{G}_2(X(T), Y(T), \Theta(T)) \end{pmatrix} \right] = \mathcal{O}(\delta^{1+k})$$

for $(X(T), Y(T), \Theta(T)) \in D_\mathcal{P} \times S^1$ (since $\partial\mathcal{H}/\partial X(X_{\mathrm{s}}, 0) = \partial\mathcal{H}/\partial Y(X_{\mathrm{s}}, 0)$=0). Thus, since $(\mathcal{P}^{T_0})^N(Q^D_{\mathrm{entr}}) = Q^D_{\mathrm{exit}} \in \partial D_\mathcal{P}$ for some N, we may conclude that the distance, measured in terms of the Hamiltonian distance function, between $W^{\mathrm{u}}_{\mathrm{out}}(P_\delta^{T_0})$ and the span $\{W^{\mathrm{s}}_{\mathrm{loc,out}}(P_\delta^{T_0}) \cup W^{\mathrm{u}}_{\mathrm{loc,out}}(P_\delta^{T_0}) \cup W^{\mathrm{s}}_{\mathrm{loc,in}}(P_\delta^{T_0}) \cup W^{\mathrm{u}}_{\mathrm{loc,in}}(P_\delta^{T_0})\} \cap D_\mathcal{P}$ at the exit point Q^D_{exit} is given by $\mathcal{M}_{\mathrm{out}}(T_0) + \mathcal{O}(\delta^k|\log\delta|)$, i.e. the same Melnikov expression (at leading order) as at the entrance point Q^D_{entr} (without any additional changes in phase, see Remark 3.6).

Since $\mathcal{M}_{\mathrm{out}}(T_0) < 0$ for all T_0, we know that $W^{\mathrm{u}}_{\mathrm{out}}(P_\delta^{T_0})$ is 'inside' $W^{\mathrm{s}}_{\mathrm{out}}(P_\delta^{T_0})$, so that the exit point Q^D_{exit} will be $\mathcal{O}(\delta)$ close to $W^{\mathrm{u}}_{\mathrm{loc,in}}(P_\delta^{T_0})$ (see Figs. 4 and 7a). The distance between $W^{\mathrm{u}}_{\mathrm{in}}(P_\delta^{T_0})$ and $W^{\mathrm{s}}_{\mathrm{in}}(P_\delta^{T_0})$ at the point Q^D_{exit} is, by definition, given by $\mathcal{M}_{\mathrm{in}}(T_0)$ (at leading order). Hence, it follows that the Melnikov function that measures the distance between $W^{\mathrm{u}}_{\mathrm{out}}(P_\delta^{T_0})$ and $W^{\mathrm{s}}_{\mathrm{in}}(P_\delta^{T_0})$ is given by

$$\mathcal{M}_{\mathrm{mixed}}(T_0) = \mathcal{M}_{\mathrm{out}}(T_0) + \mathcal{M}_{\mathrm{in}}(T_0), \tag{3.17}$$

under the condition that $\mathcal{M}_{\rm out}(T_0) < 0$ for all T_0. By (3.15) and the relation $\phi_{\rm out} = \pi - \phi_{\rm in}$ (3.16) we thus obtain

$$\mathcal{M}_{\rm mixed}(T_0) = -2\left[C\left(\pi - 2\phi_{\rm in} + \frac{6\,\tan\phi_{\rm in}}{3 + \tan^2\phi_{\rm in}}\right) + \frac{\pi\Omega^2}{\sinh k_{\rm s}\pi}(1 + {\rm e}^{k_{\rm s}\pi})\,{\rm e}^{-k_{\rm s}\phi_{\rm in}}\,\cos(\Omega T_0)\right]. \tag{3.18}$$

The same construction can be used to study the case $\mathcal{M}_{\rm in}(T_0) \neq 0$ for all T_0. Here, however, one needs to determine the path of $W^{\rm s}_{\rm in}(P_\delta^{T_0})$ through the region $D_{\mathcal{P}}$. It follows immediately that the distance between $W^{\rm s}_{\rm in}(P_\delta^{T_0})$ and $W^{\rm u}_{\rm out}(P_\delta^{T_0})$ can be expressed in *exactly the same* 'mixed' Melnikov function $\mathcal{M}_{\rm mixed}(T_0)$ that is given by (3.17) and (3.18)). See however Remark 3.6.

Remark 3.5. It should be noted that there are more examples in the literature where 'mixed' Melnikov expressions of the type considered here are derived (see for instance [2]). Nevertheless, since the system considered here does not have a special symmetric structure (chains of homoclinic orbits appear more naturally in systems with symmetries [2]), and since we have to deal here with the additional subtleties of deriving a Melnikov function in an averaged system, we decided to present a completely independent and detailed derivation of $\mathcal{M}_{\rm mixed}(T_0)$. For similar reasons, we performed an independent analysis of the passage of $W^{\rm u}_{\rm out}(P_\delta^{T_0})$ near $P_\delta^{T_0}$ and refrained from referring to general results on the passage of manifolds near another (normally hyperbolic) manifold [12,13].

Remark 3.6. By construction, the Melnikov expressions $\mathcal{M}_{\rm out}$, $\mathcal{M}_{\rm in}$ and $\mathcal{M}_{\rm mixed}$ measure the distance between stable and unstable manifolds relative to a given reference point on one of the unperturbed homoclinic orbits. Therefore, $\mathcal{M}_{\rm out}$, $\mathcal{M}_{\rm in}$ and $\mathcal{M}_{\rm mixed}$ explicitly depend on the position of that reference point on an orbit $\gamma^{\rm hom}_{\rm out}$ or $\gamma^{\rm hom}_{\rm in}$. This fact can be made explicit by taking into account the changes in the phase Θ in the computation of the Melnikov functions, see [25]. Since we have not explicitly incorporated the influence of phase differences into the Melnikov expressions, the expressions $\mathcal{M}_{\rm out}$, $\mathcal{M}_{\rm in}$, and $\mathcal{M}_{\rm mixed}$ can only be used to see whether stable and unstable manifold can intersect, and can in this form not directly be used to determine the precise location of the intersections. For instance, if the parameters in the model are such that $\mathcal{M}_{\rm out}(T_0)$ can have zeroes for certain values $T_0^{\rm int}$ of T_0 (see Section 4), then we know that $W^{\rm s}_{\rm out}(P_\delta^{T_0})$ and $W^{\rm u}_{\rm out}(P_\delta^{T_0})$ intersect transversally. However, only for $T_0 = T_0^{\rm int}$ we know the precise location of this intersection, or better, of one of the intersections: it is by construction asymptotically close to the reference point $\gamma^{\rm hom}_{\rm out}(0)$, i.e. by Section 3.2, near the Y-axis. For other values of T_0 we have to do some extra work to find the location(s) of $W^{\rm s}_{\rm out}(P_\delta^{T_0}) \cap W^{\rm u}_{\rm out}(P_\delta^{T_0})$ (we have to follow $\gamma^{\rm hom}_{\rm out}(T)$ for a time $T_0^{\rm int} - T_0$, see [25]). The precise information on the location of the intersections of the stable and unstable manifolds is not relevant for the forthcoming analysis. Nevertheless, this straightforward observation demonstrates that there indeed is a quantitative distinction between the two 'identical' expressions derived for $\mathcal{M}_{\rm mixed}(T_0)$ in the two cases considered in this section (i.e. $\mathcal{M}_{\rm out}(T_0) \neq 0$ for all T_0 and $\mathcal{M}_{\rm in}(T_0) \neq 0$ for all T_0). In the two constructions of $\mathcal{M}_{\rm mixed}(T_0)$, the reference points, relative to which the distance $\mathcal{M}_{\rm mixed}(T_0)$ is measured, are in general not the same. Therefore, the two versions of $\mathcal{M}_{\rm mixed}(T_0)$ will differ by a phase factor.

4. Chaotic behavior

In this section we interpret the outcome of the asymptotic Melnikov analysis of the previous section. It is shown that the mixed Melnikov function $\mathcal{M}_{\rm mixed}(T_0)$ plays a crucial role in the analysis of the character of the intersections of the stable and unstable manifolds of the saddle point.

Each of the three Melnikov functions defines a manifold in a three-dimensional parameter space—these parameters are related to the magnitude of the friction coefficient, the amplitude of the exterior forcing, and the frequency difference between the lunar and solar components of the forcing. Such a manifold separates the parameter space

into two regions: one in which the associated Melnikov function can have (simple) zeroes and one in which it cannot change sign. Together, these manifolds determine seven regions, one in which there are no transversal intersections, and hence no chaotic solutions, and six in which there are six different types of transversal intersections possible. Four of these six types are of a 'mixed' nature, in the sense that the chaotic solutions are 'spread out' along the full framework spanned by the outer and inner homoclinic orbits of the unperturbed limit. By a combination of the information obtained from the three Melnikov functions with geometrical arguments based on the nearly integrable character of the weakly forced system, it is possible to deduce the structure of all stable and unstable manifolds of the saddle point of the Poincaré map (and their intersections) and to construct various horseshoe maps in all six 'chaotic' regions.

4.1. Transversal intersections

The three Melnikov functions $\mathcal{M}_{\rm in}(T_0)$, $\mathcal{M}_{\rm out}(T_0)$ and $\mathcal{M}_{\rm mixed}(T_0)$ define the three critical manifolds, $\mathcal{C}_{\rm out}$, $\mathcal{C}_{\rm in}$ and $\mathcal{C}_{\rm mixed}$ in the (Ω, F, C)-parameter space (with $C > 0$ and $-(4/9)\sqrt{3} < F < 0$, see Section 3.2). The definition of these manifolds is straightforward: they separate the regions in (Ω, F, C)-parameter space where $\mathcal{M}_{\rm in}(T_0)$, $\mathcal{M}_{\rm out}(T_0)$, $\mathcal{M}_{\rm mixed}(T_0)$ can have zeroes, from those where the Melnikov functions do not change sign as a function of T_0. It follows immediately from the structure of the expressions in (3.15) and (3.18) that the manifolds $\mathcal{C}_{\rm out,in,mixed}$ can be expressed in terms of a function $C = C_{\rm out,in,mixed}(\Omega, F)$, so that $\mathcal{M}_{\rm out,in,mixed}(T_0)$ has countably many (simple) zeroes as function of T_0 for $0 < C < C_{\rm out,in,mixed}(\Omega, F)$, and no zeroes for $C > C_{\rm out,in,mixed}(\Omega, F)$; $\mathcal{C}_{\rm out,in,mixed}$ are given by

$$
\begin{aligned}
\mathcal{C}_{\rm out} &= \left\{ C = C_{\rm out}(\Omega, F) = \left| \frac{\pi \Omega^2}{\sinh k_{\rm s}\pi} \mathrm{e}^{k_{\rm s}\phi_{\rm out}} \left(\phi_{\rm out} - \frac{3 \tan \phi_{\rm out}}{3 + \tan^2 \phi_{\rm out}} \right)^{-1} \right| \right\}, \\
\mathcal{C}_{\rm in} &= \left\{ C = C_{\rm in}(\Omega, F) = \left| \frac{\pi \Omega^2}{\sinh k_{\rm s}\pi} \mathrm{e}^{-k_{\rm s}\phi_{\rm in}} \left(-\phi_{\rm in} + \frac{3 \tan \phi_{\rm in}}{3 + \tan^2 \phi_{\rm in}} \right)^{-1} \right| \right\}, \\
\mathcal{C}_{\rm mixed} &= \left\{ C = C_{\rm mixed}(\Omega, F) = \left| \frac{\pi \Omega^2}{\sinh k_{\rm s}\pi} (1 + \mathrm{e}^{k_{\rm s}\pi}) \mathrm{e}^{-k_{\rm s}\phi_{\rm in}} \left(\pi - 2\phi_{\rm in} + \frac{6 \tan \phi_{\rm in}}{3 + \tan^2 \phi_{\rm in}} \right)^{-1} \right| \right\}
\end{aligned}
\tag{4.1}
$$

(recall that $\phi_{\rm out,in} = \phi_{\rm out,in}(F)$ (B.6), $k_{\rm s} = k_{\rm s}(\Omega, F)$ (B.7)). The manifold $\mathcal{C}_{\rm mixed}$ is only defined in the region $\{C > C_{\rm out}\} \cup \{C > C_{\rm in}\}$ (Section 3.4).

All three manifolds $\mathcal{C}_{\rm out}$, $\mathcal{C}_{\rm in}$ and $\mathcal{C}_{\rm mixed}$ vanish as $\Omega \to 0$. In this limit there is no forcing term in (3.12), so that there can be no transversal intersections of stable and unstable manifolds. Note, by (3.2) and (3.5), that $\Omega = 0$ corresponds to the periodically forced case (Section 3.2). Similar behavior occurs for tidal frequencies ω and $\omega_{\rm sol}$ (3.2) that are not both close to the same resonance, i.e. when $|\Omega| \gg 1$. This is because the term $\sinh(k_{\rm s}\pi)$ in the denominators of the expressions in (4.1) dominates all other terms as $k_{\rm s} = \Omega/2\mu \to \pm\infty$ (B.7). Thus, we conclude that there can only be non-trivial (i.e. chaotic) behavior in system (3.12) when the frequencies of the 'lunar' and 'solar' components of the external forcing term (3.2) are not identical, and close to resonance.

There are two other relevant limits: $F \uparrow 0$ and $F \downarrow -(4/9)\sqrt{3}$. The limit $F \uparrow 0$ corresponds by (B.6) to $\phi_{\rm out} \downarrow \pi/2$ and $\phi_{\rm in} \uparrow \pi/2$. It follows from (B.5) that $\mu \downarrow 0$ as $\phi_{\rm out,in} \to \pi/2$, so that, by (B.7), all three manifolds $\mathcal{C}_{\rm out,in,mixed}$ approach $\{C = 0\}$ exponentially fast as $F \uparrow 0$, due to the dominating exponential growth of the term $\sinh(k_{\rm s}\pi)$ in the denominators in (4.1). Hence, also in this limit, all non-trivial behavior vanishes. Note that in the integrable limit system (i.e. $\delta = \varepsilon = 0$ in (3.12)), the inner and outer homoclinic orbit merge as $F \uparrow 0$ (both $\gamma_{\rm out}^{\rm hom}$ and $\gamma_{\rm in}^{\rm hom}$ coincide with the degenerate circle of fixed points $\{X^2 + Y^2 = 1\}$ when $F = 0$). This also implies that $\mathcal{M}_{\rm out}(T_0)$ and $\mathcal{M}_{\rm in}(T_0)$ must measure the same splitting distance in this limit, except for a change in sign, since the

local stable manifold segment of $\gamma_{\text{out}}^{\text{hom}}$ merges with the local unstable manifold segment of $\gamma_{\text{out}}^{\text{hom}}$ and vice versa. This is confirmed by (3.15): $\mathcal{M}_{\text{out,in}}(T_0) \to \mp\pi C$ as $F \uparrow 0$. It thus follows that $\mathcal{M}_{\text{mixed}}(T_0) \to 0$ for $F \uparrow 0$ (3.17). However, this has no influence on the existence of 'mixed' intersections in this limit (due to the exponential decay of $C_{\text{mixed}}(\Omega, F)$ (4.1)).

A similar geometrical point of view gives additional insight in the limit $F \downarrow -(4/9)\sqrt{3}$ that corresponds to $\phi_{\text{out}} \uparrow \pi$ and $\phi_{\text{in}} \downarrow 0$. In the integrable limit, $\gamma_{\text{in}}^{\text{hom}}$ shrinks to a point as $F \downarrow -(4/9)\sqrt{3}$, while $\gamma_{\text{out}}^{\text{hom}}$ reaches a well-defined limit. Once again we find that the structure of the manifolds $\mathcal{C}_{\text{out,in,mixed}}$ is dominated by the exponential growth of $\sinh(k_s\pi)$ (since again $\mu \to 0$ as $\phi_{\text{out,in}} \to \pi, 0$ (B.5)). However, one must be careful in interpreting the behavior of the Melnikov function $\mathcal{M}_{\text{in}}(T_0)$ for the shrinking orbit $\gamma_{\text{in}}^{\text{hom}}$. A leading order asymptotic analysis yields that

$$C_{\text{in}}(\Omega, \varphi) = \frac{45\pi\Omega^2}{2\varphi^5} \mathrm{e}^{-(3|\Omega|/2\varphi)(\pi+\varphi)}(1 + \mathcal{O}(\varphi^2)) \quad \text{for } 0 < \varphi = \phi_{\text{in}} \ll 1. \tag{4.2}$$

Thus, $C_{\text{in}}(\Omega, \varphi)$ indeed decays exponentially as $\varphi \downarrow 0$ for a given fixed value of Ω. However, the exponential decay is not uniform in Ω, the limit of $C_{\text{in}}(\Omega, \varphi)$ for $(\Omega, \varphi) \to (0, 0)$ does not exist (consider for instance $\Omega = w\varphi$ for fixed w: $C_{\text{in}}(w\varphi, \varphi)$ behaves as $1/\varphi^3$ for $0 < \varphi \ll 1$ (4.2)). Hence, the manifold $\mathcal{C}_{\text{in}}$ has a singularity at $(\Omega, F) = (0, -(4/9)\sqrt{3})$ and becomes unbounded near this point, see Fig. 5.

Note that the existence of a singularity on $\mathcal{C}_{\text{in}}$ also implies that it is possible to have transversal intersections of $W_{\text{in}}^{\text{s}}(P_\delta^{T_0})$ and $W_{\text{in}}^{\text{u}}(P_\delta^{T_0})$ for arbitrarily large values of the friction parameter C, since any C will be below $\mathcal{C}_{\text{in}}$ for appropriately chosen values of Ω and F. This is quite a surprising and counter-intuitive result. However, all elements of $W_{\text{in}}^{\text{s}}(P_\delta^{T_0}) \cap W_{\text{in}}^{\text{u}}(P_\delta^{T_0})$ will be close to the now 'arbitrarily small' orbit $\gamma_{\text{in}}^{\text{hom}}$ and thus to the saddle point $P_\delta^{T_0}$. Moreover, in order to retain the validity of the approach, it is necessary to assume that $C = \mathcal{O}(1)$ with respect to δ. This implies that one has to choose δ (and thus ε) 'small enough' when one wants to consider C 'large'.

Parameter combinations (Ω, F, C) that are above all three manifolds $\mathcal{C}_{\text{out}}$, $\mathcal{C}_{\text{in}}$ and $\mathcal{C}_{\text{mixed}}$, i.e. $C > C_{\text{out,in,mixed}}(\Omega, F)$, correspond to 'trivial' flows in (3.12), in the sense that there are no intersections of the stable and unstable manifolds to the saddle $P_\delta^{T_0}$ of the Poincaré map $\mathcal{P}^{T_0}$. The region below the manifolds $\mathcal{C}_{\text{out}}$, $\mathcal{C}_{\text{in}}$ and $\mathcal{C}_{\text{mixed}}$ can a priori be divided into six subregions (see Fig. 5):

- *Double chaos*: $C < \min(C_{\text{out}}(\Omega, F), C_{\text{in}}(\Omega, F))$. In this region both $\mathcal{M}_{\text{out}}(T_0)$ and $\mathcal{M}_{\text{in}}(T_0)$ have (countably many) simple zeroes, so that there are transversal intersections of both $W_{\text{out}}^{\text{s}}(P_\delta^{T_0})$ with $W_{\text{out}}^{\text{u}}(P_\delta^{T_0})$ and of $W_{\text{in}}^{\text{s}}(P_\delta^{T_0})$ with $W_{\text{in}}^{\text{u}}(P_\delta^{T_0})$. The manifold $\mathcal{C}_{\text{mixed}}$ is not defined in this region (Section 3.4), but, as we shall show in the next section, both $W_{\text{out}}^{\text{s}}(P_\delta^{T_0}) \cap W_{\text{in}}^{\text{u}}(P_\delta^{T_0}) \neq \emptyset$ and $W_{\text{in}}^{\text{s}}(P_\delta^{T_0}) \cap W_{\text{out}}^{\text{u}}(P_\delta^{T_0}) \neq \emptyset$, see Fig. 7d. This region consists of two components, one on either side of the plane $\{\Omega = 0\}$.
- *Inner chaos*: $\max(C_{\text{out}}(\Omega, F), C_{\text{mixed}}(\Omega, F)) < C < C_{\text{in}}(\Omega, F)$. Here only $\mathcal{M}_{\text{in}}(T_0)$ has zeroes, so that there can only be transversal intersections of $W_{\text{in}}^{\text{s}}(P_\delta^{T_0})$ and $W_{\text{in}}^{\text{u}}(P_\delta^{T_0})$. Due to the singular behavior of $\mathcal{C}_{\text{in}}$ for (Ω, F) near $(0, -(4/9)\sqrt{3})$, this region, which again consists of two components, is the largest of the 6 regions, i.e. inner chaos is the most common type of chaos in this system.
- *Outer chaos*: $\max(C_{\text{in}}(\Omega, F), C_{\text{mixed}}(\Omega, F)) < C < C_{\text{out}}(\Omega, F)$. This region turns out to be empty: there are no parameter combinations for which only $W_{\text{out}}^{\text{s}}(P_\delta^{T_0})$ and $W_{\text{out}}^{\text{u}}(P_\delta^{T_0})$, and none of the other combinations, have intersections (see Remark 4.1).
- *Mixed chaos*: $\max(C_{\text{out}}(\Omega, F), C_{\text{in}}(\Omega, F)) < C < C_{\text{mixed}}(\Omega, F)$. This region consists of one component with $\Omega > 0$. In this region there are no 'classical' intersections, i.e. when one considers either the perturbations of $\gamma_{\text{out}}^{\text{hom}}$ or those of $\gamma_{\text{in}}^{\text{hom}}$ separately (as was done in [15,17,26]), one will conclude that there are no 'non-trivial' solutions (see Remark 4.1). However, $\mathcal{M}_{\text{mixed}}(T_0)$ has simple zeroes in this region, so that $W_{\text{out}}^{\text{u}}(P_\delta^{T_0})$ and $W_{\text{in}}^{\text{s}}(P_\delta^{T_0})$ intersect transversally. Like in the classical case [9,25], these intersections can of course be related to a Smale horseshoe map, as we shall see in the next section.

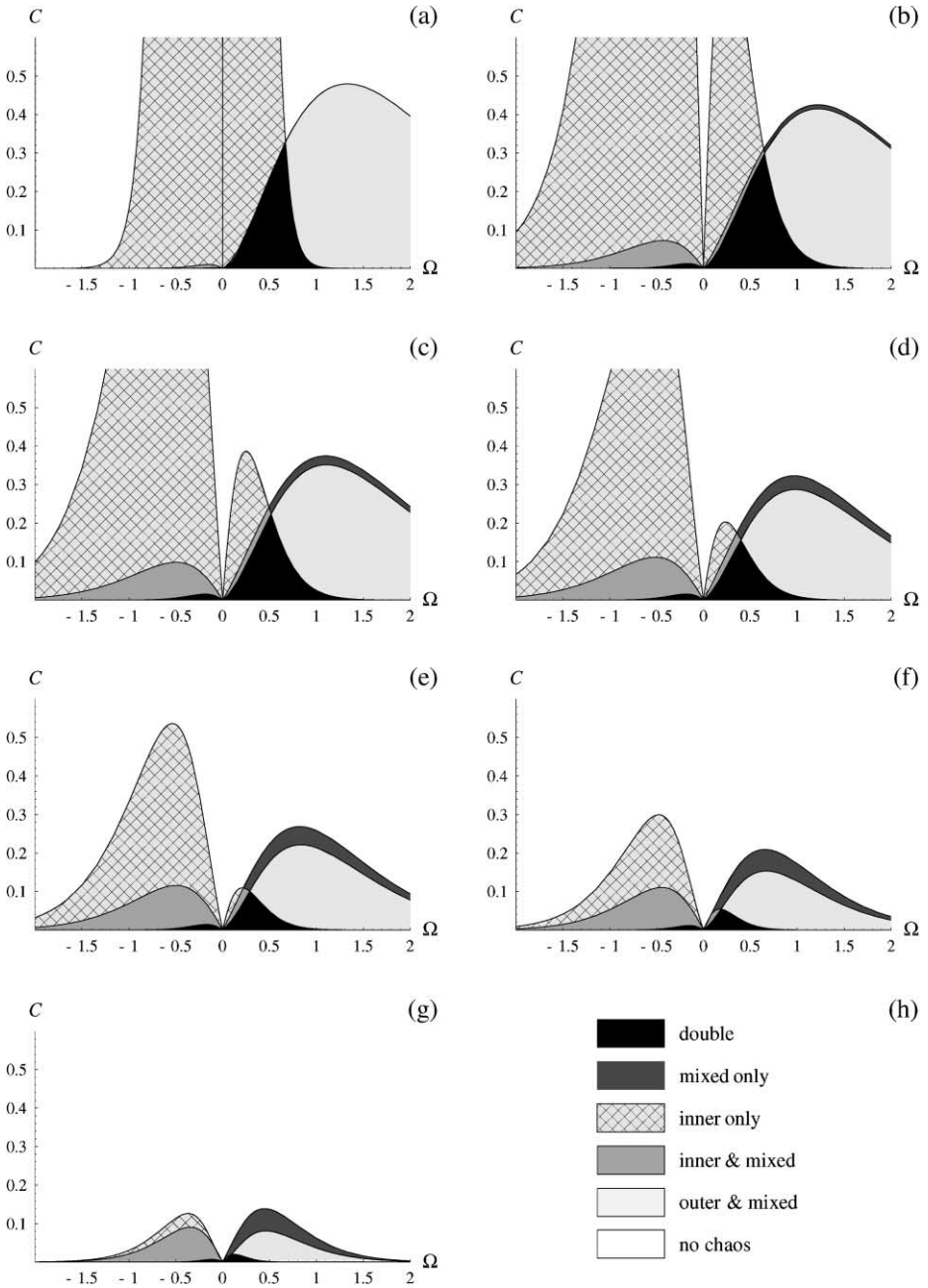

Fig. 5. Intersections of the manifolds $\mathcal{C}_{\text{out}}$, $\mathcal{C}_{\text{in}}$ and $\mathcal{C}_{\text{mixed}}$ with various equally spaced $\{F = F_i\}$ planes, where $F_i = 0.01 - (4/9)\sqrt{3} \times (1 - (1/7)(i - 1)) \in (-(4/9)\sqrt{3}, 0)$, $i = 1, \ldots, 7$. These manifolds determine the various types of chaos described in this section. Note that the 'outer chaos' case does not exist.

- *Inner and mixed chaos*: $C_{\text{out}}(\Omega, F) < C < \min(C_{\text{in}}(\Omega, F), C_{\text{mixed}}(\Omega, F))$. Here, there are 'classical' intersections of $W^{\text{s}}_{\text{in}}(P^{T_0}_\delta)$ and $W^{\text{u}}_{\text{in}}(P^{T_0}_\delta)$, while $\mathcal{M}_{\text{out}}(T_0) \neq 0$ for all T_0, so that $\mathcal{M}_{\text{mixed}}(T_0)$ can be constructed; $\mathcal{M}_{\text{mixed}}(T_0)$ also has zeroes, which implies that $W^{\text{u}}_{\text{in}}(P^{T_0}_\delta)$ also intersects $W^{\text{s}}_{\text{out}}(P^{T_0}_\delta)$ transversally (see Fig. 7c). This region consists of two components, one on either side of the plane $\{\Omega = 0\}$.
- *Outer and mixed chaos*: $C_{\text{in}}(\Omega, F) < C < \min(C_{\text{out}}(\Omega, F), C_{\text{mixed}}(\Omega, F))$. This region consists of one component with $\Omega > 0$ that is close, but just below, the 'mixed chaos' component. There are classical, outer transversal intersections and mixed intersections of $W^{\text{u}}_{\text{out}}(P^{T_0}_\delta)$ and $W^{\text{s}}_{\text{in}}(P^{T_0}_\delta)$.

Remark 4.1. The fact that a quasi-periodic forcing term with two 'nearby' frequencies can create chaotic behavior of the small amplitude solutions of a weakly forced nonlinear oscillator was already noted in [15,26]. However, in these papers no attention has been paid to the possibility of mixed intersections, or to the construction of a mixed Melnikov function $\mathcal{M}_{\text{mixed}}(T_0)$. As a consequence, neither of the 'mixed' types of chaos have been discussed in these papers. Therefore, the existence of the 'mixed chaos' region is of particular interest, since in this region in parameter space there is chaotic behavior, while the 'classical' Melnikov functions do not change sign. Furthermore, the 'mixed' Melnikov analysis also shows that it is not possible to have 'classical' 'outer chaos' without mixed intersections.

4.2. The structure of $W^{s,u}_{out,in}(P^{T_0}_\delta)$ and the construction of horseshoe maps

Since the Poincaré map $\mathcal{P}^{T_0}$ is based on the weakly perturbed integrable flow generated by (3.12), it is possible to obtain a geometric, *qualitative* insight in the structure of the manifolds $W^{\text{s}}_{\text{out}}(P^{T_0}_\delta)$, $W^{\text{u}}_{\text{out}}(P^{T_0}_\delta)$, $W^{\text{s}}_{\text{in}}(P^{T_0}_\delta)$, and $W^{\text{u}}_{\text{in}}(P^{T_0}_\delta)$ in all different cases distinguished in the previous section. Based on the behavior of the three Melnikov functions and some fundamental properties of homoclinic tangles, it is possible to sketch a qualitative picture of the stable and unstable manifolds. The following three properties are especially useful (see [9,25]):

- Once two manifolds intersect in a so-called 'pip', a 'primary intersection point' (see [20,25] and Remark 4.2), they must intersect in countably infinitely many pips. Adjacent pips form an ordered sequence along the manifolds.
- Near the saddle point the amplitude of the 'lobes' ([20,25] and Remark 4.2) increases. This is a consequence of the fact that the pips accumulate on the saddle point $P^{T_0}_\delta$, while the area of a lobe is, at leading order, conserved (the map $\mathcal{P}^{T_0}$ is (also) almost Hamiltonian and thus almost area-preserving, where 'almost' means: up to $\mathcal{O}(\delta)$ perturbations).
- The map $\mathcal{P}^{T_0}$ maps a pair of two adjoining lobes to the next adjoining pair of lobes. Thus, also intersections of lobes are mapped to intersections of lobes (i.e. if two lobes intersect, their images and pre-images must also intersect).

The structure of the manifolds $W^{\text{s,u}}_{\text{out,in}}(P^{T_0}_\delta)$ can now be obtained for all cases by a strict application of the above properties, in combination with the character of the leading order, integrable flow. See Fig. 6 for the 'classical' 'inner chaos' case and Fig. 7 for the four 'mixed' cases.

Note in particular, that it now follows that there must also be 'mixed' intersections in the 'double chaos' case, i.e. in this case $W^{\text{u}}_{\text{out}}(P^{T_0}_\delta) \cap W^{\text{s}}_{\text{in}}(P^{T_0}_\delta) \neq \emptyset$, but also $W^{\text{s}}_{\text{out}}(P^{T_0}_\delta) \cap W^{\text{u}}_{\text{in}}(P^{T_0}_\delta) \neq \emptyset$ (see Fig. 7d) To see this, we consider the lobes formed by $W^{\text{s}}_{\text{out}}(P^{T_0}_\delta)$ and $W^{\text{u}}_{\text{loc,out}}(P^{T_0}_\delta)$, near $P^{T_0}_\delta$ (these exist, since $\mathcal{M}_{\text{out}}(T_0)$ has zeroes). These lobes become longer and thinner the closer the pips approach $P^{T_0}_\delta$, and are 'folded' along the two branches of the stable manifold of $P^{T_0}_\delta$, $W^{\text{s}}_{\text{out}}(P^{T_0}_\delta)$ and $W^{\text{s}}_{\text{in}}(P^{T_0}_\delta)$. Since $\mathcal{M}_{\text{in}}(T_0)$ also has zeroes, there will also be lobes formed by $W^{\text{u}}_{\text{in}}(P^{T_0}_\delta)$ and $W^{\text{s}}_{\text{loc,in}}(P^{T_0}_\delta)$ near $P^{T_0}_\delta$. These lobes will be folded along $W^{\text{u}}_{\text{out}}(P^{T_0}_\delta)$ and $W^{\text{u}}_{\text{in}}(P^{T_0}_\delta)$. The lobes 'inside', i.e. those that accumulate on $W^{\text{u}}_{\text{in}}(P^{T_0}_\delta)$ will form the 'standard' homoclinic tangle with the lobes of $W^{\text{s}}_{\text{in}}(P^{T_0}_\delta)$ and $W^{\text{u}}_{\text{loc,in}}(P^{T_0}_\delta)$. The lobes 'outside', i.e. those that accumulate on $W^{\text{u}}_{\text{out}}(P^{T_0}_\delta)$ will have countably many

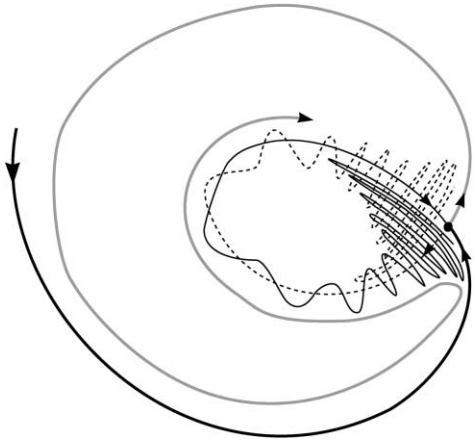

Fig. 6. A sketch of the stable and unstable manifolds to $P_\delta^{T_0}$ in the 'inner chaos' case. The 'color coding' of the manifolds is the same as in Fig. 4.

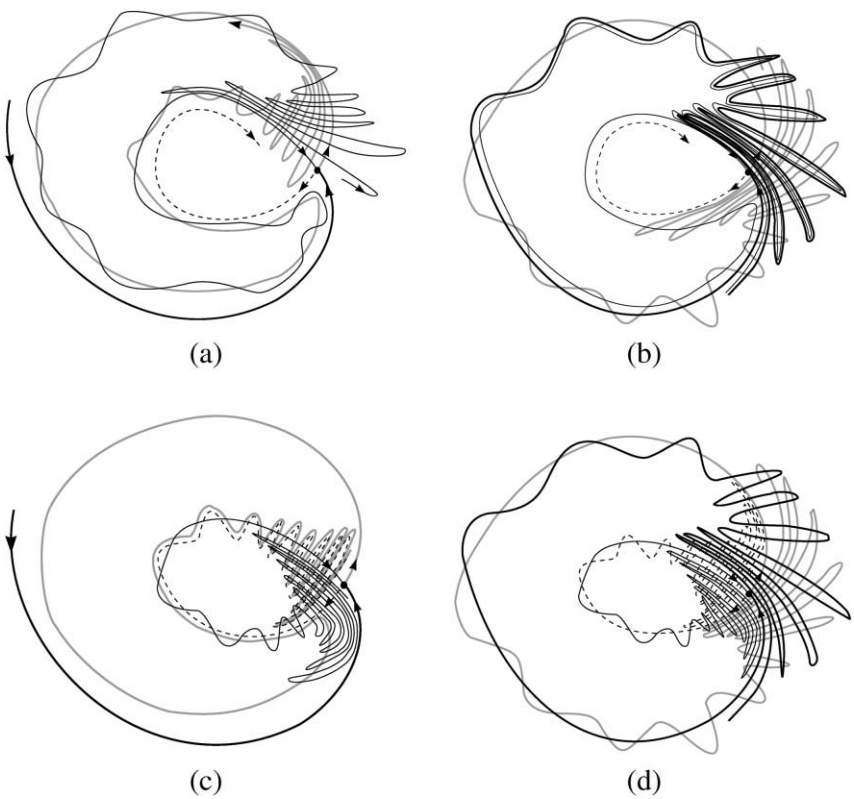

Fig. 7. The sketches of (the intersections of) the stable and unstable manifolds for the four 'mixed' types: (a) mixed chaos; (b) outer and mixed chaos; (c) inner and mixed chaos; (d) double chaos. The 'color coding' of the manifolds is the same as in Fig. 4.

intersections with the 'inside' lobes of $W^{\mathrm{s}}_{\mathrm{out}}(P_\delta^{T_0})$ and $W^{\mathrm{u}}_{\mathrm{loc,out}}(P_\delta^{T_0})$, i.e. those lobes that accumulate on $W^{\mathrm{s}}_{\mathrm{in}}(P_\delta^{T_0})$, near $P_\delta^{T_0}$, since $W^{\mathrm{u}}_{\mathrm{out}}(P_\delta^{T_0})$ and $W^{\mathrm{s}}_{\mathrm{in}}(P_\delta^{T_0})$ both originate from, or limit on, $P_\delta^{T_0}$. Hence, there are countably many intersections of $W^{\mathrm{s}}_{\mathrm{out}}(P_\delta^{T_0})$ and $W^{\mathrm{u}}_{\mathrm{in}}(P_\delta^{T_0})$. Likewise, it follows that $W^{\mathrm{u}}_{\mathrm{out}}(P_\delta^{T_0})$ and $W^{\mathrm{s}}_{\mathrm{in}}(P_\delta^{T_0})$ also have countably many intersections (Fig. 7d).

Transversal intersections of stable and unstable manifolds imply that certain Nth iterates of the map $\mathcal{P}^{T_0}$ must have an invariant hyperbolic Cantor set Λ. Restricted to Λ, the iterated map $(\mathcal{P}^{T_0})^N$ is topologically equivalent to a shift map on a finite number of symbols. This is in essence the statement of the Smale–Birkhoff theorem [9,25]. The key ingredient to the proof of the Smale–Birkhoff theorem is the construction of a horseshoe map from a map that has a hyperbolic fixed point p (here $P_\delta^{T_0}$) with stable and unstable manifolds that intersect transversally in a point q (here: a zero of either $\mathcal{M}_{\mathrm{out}}(T_0)$, $\mathcal{M}_{\mathrm{in}}(T_0)$ or $\mathcal{M}_{\mathrm{mixed}}(T_0)$).

In the cases that only one of the Melnikov functions has zeroes, i.e. the 'inner chaos' and the 'mixed chaos' case (recall that (only) 'outer chaos' does not exist), the construction of the horseshoe map is identical to that in the standard case. In order to explain the difference between these two standard cases and the other three more complex cases ('mixed and outer chaos', 'mixed and inner chaos' and 'double chaos') we give a rough sketch of the construction of a horseshoe map, and the associated intersections of the stable and unstable manifolds, for the most common type, the 'inner chaos' (Fig. 6).

Assume that $q \in W^{\mathrm{s}}_{\mathrm{in}}(P_\delta^{T_0}) \cap W^{\mathrm{u}}_{\mathrm{in}}(P_\delta^{T_0})$ and that q is a pip. Consider a quadrangle $\mathcal{V} \subset D_{\mathcal{P}}$ with $P_\delta^{T_0} \in \mathcal{V}$, such that $\partial\mathcal{V} = \partial\mathcal{V}^s_{\mathrm{out}} \cup \partial\mathcal{V}^u_{\mathrm{out}} \cup \partial\mathcal{V}^s_{\mathrm{in}} \cup \partial\mathcal{V}^u_{\mathrm{in}}$ with $W^{\mathrm{s,u}}_{\mathrm{loc,out,in}}(P_\delta^{T_0}) \cap \partial\mathcal{V} \in \partial\mathcal{V}^{\mathrm{s,u}}_{\mathrm{out,in}}$. The map $\mathcal{P}^{T_0}$ will stretch $\mathcal{V}$ in the direction of the unstable manifolds, and squeeze $\mathcal{V}$ in the direction of the stable manifolds. Thus, $\partial\mathcal{V}^u_{\mathrm{in}}$ is mapped by $\mathcal{P}^{T_0}$ towards q along $W^{\mathrm{u}}_{\mathrm{in}}(P_\delta^{T_0})$ and $\partial\mathcal{V}^s_{\mathrm{in}}$ is mapped by the inverse, $(\mathcal{P}^{T_0})^{-1}$, towards q along $W^{\mathrm{s}}_{\mathrm{in}}(P_\delta^{T_0})$. We define k and ℓ as the minimal numbers such that $q \in (\mathcal{P}^{T_0})^k(\mathcal{V})$ and $q \in (\mathcal{P}^{T_0})^{-\ell}(\mathcal{V})$. Now, the map $(\mathcal{P}^{T_0})^N$, with $N = k + \ell$, acts as the classical horseshoe map on the region $\mathcal{V}_{\mathrm{hs}} = (\mathcal{P}^{T_0})^{-\ell}(\mathcal{V})$: $(\mathcal{P}^{T_0})^N$ stretches, squeezes and bends $\mathcal{V}_{\mathrm{hs}}$ so that $(\mathcal{P}^{T_0})^N(\mathcal{V}_{\mathrm{hs}}) \cap \mathcal{V}_{\mathrm{hs}} = (\mathcal{P}^{T_0})^k(\mathcal{V}) \cap (\mathcal{P}^{T_0})^{-\ell}(\mathcal{V})$ consists of two 'strips', one containing $P_\delta^{T_0}$, the other q (see [9,25] for all details of this construction).

The region $\mathcal{V}$ is stretched by $\mathcal{P}^{T_0}$ along both $W^{\mathrm{u}}_{\mathrm{in}}(P_\delta^{T_0})$ and $W^{\mathrm{u}}_{\mathrm{out}}(P_\delta^{T_0})$, but the standard horseshoe construction does not pay attention to the 'outer' parts of $(\mathcal{P}^{T_0})^k(\mathcal{V}) = (\mathcal{P}^{T_0})^N(\mathcal{V}_{\mathrm{hs}})$ (that has $(\mathcal{P}^{T_0})^k(\partial\mathcal{V}^u_{\mathrm{out}})$ as 'tip'). Likewise, the outer part of $\mathcal{V}_{\mathrm{hs}}$ (that has $(\mathcal{P}^{T_0})^{-\ell}(\partial\mathcal{V}^s_{\mathrm{out}})$ as 'tip'), has also not been considered. This was of course not necessary, since it is assumed that there are no other intersections than those of the inner stable and unstable manifolds: the 'outer' parts of $\mathcal{V}_{\mathrm{hs}}$ and $(\mathcal{P}^{T_0})^N(\mathcal{V}_{\mathrm{hs}})$ are irrelevant to the dynamics in this case.

This changes drastically in the 'outer and mixed chaos', 'inner and mixed chaos' and 'double chaos' cases. In Fig. 8 we have sketched a construction of a horseshoe map for the 'outer and mixed chaos' case. The main difference with the above standard case is that here both stable manifolds have intersections with the unstable outer manifold. Thus, we can now 'tune' the region $\mathcal{V}$ and k, ℓ such that $(\mathcal{P}^{T_0})^N(\mathcal{V}_{\mathrm{hs}}) \cap \mathcal{V}_{\mathrm{hs}} = (\mathcal{P}^{T_0})^k(\mathcal{V}) \cap (\mathcal{P}^{T_0})^{-\ell}(\mathcal{V})$ for instance consists of three strips. It follows that the map $(\mathcal{P}^{T_0})^N$ defines an invariant hyperbolic set Λ on $\mathcal{V}$ on which $(\mathcal{P}^{T_0})^N$ is equivalent to a shift on 3 symbols (the details of this statement can be checked by the standard theory presented in [9,25]).

Of course the fact that $(\mathcal{P}^{T_0})^N$ is equivalent to a shift in 3 symbols, instead of the classical example of the horseshoe map that is equivalent to a shift on 2 symbols, is not special: the classical horseshoe construction sketched above (for the 'inner chaos' case), can be modified so that it yields a horseshoe map that is equivalent (on an invariant set Λ) to a shift on n symbols, for any $n \geq 2$ (this can be achieved by stretching $\mathcal{V}_{\mathrm{hs}}$ further along $W^{\mathrm{s}}_{\mathrm{in}}(P_\delta^{T_0})$, so that $\mathcal{V}_{\mathrm{hs}} \cup W^{\mathrm{u}}_{\mathrm{in}}(P_\delta^{T_0})$ consists of more than two components). However, in the 'inner chaos' case, periodic and/or chaotic points of the map $\mathcal{P}^{T_0}$ (see Remark 4.3) can only be found in an $\mathcal{O}(\sqrt{\delta})$ neighborhood of the unperturbed inner homoclinic orbit $\gamma^{\mathrm{hom}}_{\mathrm{in}}$ (note that the $\mathcal{O}(\sqrt{\delta})$ estimate comes from the behavior of $\mathcal{P}^{T_0}$ near the saddle point $P_\delta^{T_0}$). It follows from the construction of the horseshoe map for the 'outer and mixed chaos' case (Fig. 7b and Fig. 8) that

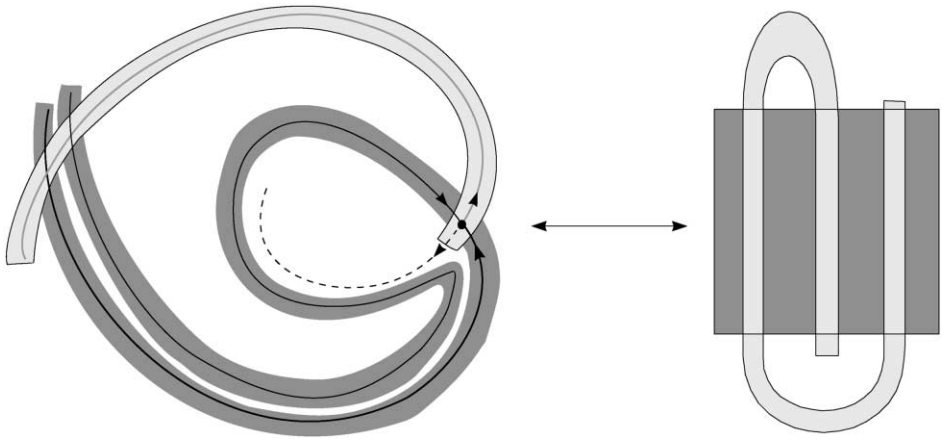

Fig. 8. A construction of a horseshoe map for the 'outer and mixed chaos' case. The second map can be obtained from the first by a topological deformation.

the periodic and/or chaotic points of the map $\mathcal{P}^{T_0}$ occur in an $\mathcal{O}(\sqrt{\delta})$ neighborhood of the union $\gamma_{\text{out}}^{\text{hom}} \cup \gamma_{\text{in}}^{\text{hom}}$ of the unperturbed and outer and inner homoclinic orbits. The same is true for the 'inner and mixed chaos' and 'double chaos' cases. In these three cases, the chaotic solutions to (3.12) are 'spread out' over an $\mathcal{O}(\sqrt{\delta})$ neighborhood of $\{\gamma_{\text{out}}^{\text{hom}} \cup \gamma_{\text{in}}^{\text{hom}}\} \times S^1$.

Remark 4.2. The 'pip' and 'lobe' terminology is based on [20], see also [25]. Let p be a saddle point of a planar map $\mathcal{P}$, with stable/unstable manifolds $W^{\text{s,u}}(p)$. Let $q \in W^{\text{s}}(p) \cap W^{\text{u}}(p)$ and let $S[p, q]$, respectively $U[p, q]$, denote the segment of $W^{\text{s}}(p)$, respectively. $W^{\text{u}}(p)$, from p to q (including p and q); q is called a primary intersection point, a 'pip', if $S[p, q] \cap U[p, q] = \{p \cup q\}$. Let q_1 and q_2 be two adjacent pips, i.e. there are no other pips on the segments $S[q_1, q_2] \subset W^s(p)$ and $U[q_1, q_2] \subset W^u(p)$. The region bounded by $S[q_1, q_2]$ and $U[q_1, q_2]$ is called a lobe.

Remark 4.3. A chaotic point of the map $\mathcal{P}^{T_0}$ corresponds to an element ρ of the invariant (Cantor) set Λ of a map $(\mathcal{P}^{T_0})^N$ (for a certain N) by a horseshoe map construction as sketched above. On Λ, $(\mathcal{P}^{T_0})^N$ is equivalent to a shift map on the space of bi-infinite sequences of n symbols (for a certain n). The fact that ρ is chaotic implies that ρ corresponds to a 'random' (bi-infinite) sequence [9,25].

5. Discussion

We have shown that the tidal elevation within an almost-enclosed short basin that is connected to a sea by a narrow strait may respond chaotically to the forcing of an exterior tide with lunar and solar components. We have focused on the role played by the geometry of the basin and the interactions between the nonlinearities induced by the geometry and the special structure of the quasi-periodic forcing term. We have established that this interaction generates various essentially different types of chaotic behavior.

There are many reports in the literature of 'irregular' tidal oscillations [3,7,10,14]; in [6,24] the 'irregularity' is measured by analyzing time series of observations and determining an estimate of the (embedding) dimension of the data. These observations, however, do not necessarily imply that the 'irregularity' of the tidal oscillations are due to nonlinearity associated with the geometry of the basin, i.e. the mechanism studied in this paper. Nevertheless,

our study implies that almost-enclosed basins in the coastal zone may respond chaotically to forcing by a combination of semi-diurnal solar and lunar tides, when both are close to resonance. This may express itself through spectral peak-broadening, noisiness of tidal 'constants' (amplitudes and phases of astronomically determined tidal frequencies), and irregular subsequent elevation extrema [6,17,24]. A related mechanism may be operating when not the tide itself, but one of the higher order modes is in resonance with the basin. Such a situation may appear in fjords, that typically have Helmholtz periods of a couple of minutes to an hour [11]. For this situation a modulation equation can be derived that is remarkably similar to (3.8) [17]. This equation can be studied and classified by the same (mixed) Melnikov functions in combination with the geometric approach of Section 4. In a case like this, the chaotic response manifests itself by secondary elevation changes [10] and may actually be amplified in the accompanying current field [7,17].

It should be remarked that the model (1.1) studied in this paper is overly simplified. The derivation (1.1) is based on several assumptions that can be considered to be unrealistic in many natural basins [16]. For instance, many basins cannot be considered to be connected to the sea by a narrow strait. The model also neglects the nonlinear character of the flow through the channel. From a physical point of view, the assumption of weak friction employed in the model is particularly questionable. On the other hand, it is quite interesting in this respect that 'inner chaos' can, for idealized cases, be reached for arbitrarily large values of the friction parameter (Section 4.1 and Fig. 5). In work in progress [23] the tidal dynamics of half-open bays is studied. Here, modulation equations like (3.8), i.e. equations that may exhibit chaotic behavior, are obtained directly from the full hydrodynamic equations that govern the flow in such a basin. This implies that the analysis of this paper is also relevant in this much more realistic and general context.

Moreover, we note that on longer than fortnightly time scales, slow modulation of environmental conditions (such as mean sea level, tidal forcing amplitudes, basin shape) may bring a basin into or out of resonance. This may provoke relatively drastic shifts in the basin's response to the tidal forcing. This phenomenon can be accounted for by the theory developed here, and in [16,17]: the parameters in (3.8) will change under these environmental conditions and the drastic shifts will be triggered by bifurcations, for instance of saddle node type, in (3.8) (see [16,17] for more details). Therefore, the ideas of nonlinear tidal dynamics developed in [16,17] and this paper may be relevant to explain certain changes in sedimentation records [18].

There are also some important mathematical issues we did not discuss in this paper. First of all, there is the problem of the existence of chaotic *attractors*. We have only shown the existence of chaotic solutions, but, these solutions cannot be stable, due to the stretch and squeeze character of their construction. This is, of course, a fundamental issue and is not special for the Helmholtz oscillator. It was found in [17] by numerical simulations that there are chaotic attractors, both in the averaged system and the underlying system (1.1), when δ is increased to values that can no longer be considered to be asymptotically small. This behavior is typical for forced nonlinear oscillators [9,25].

Another important fundamental problem we did not yet touch upon is the implication of the existence of chaotic solutions in the averaged system for the underlying system (1.1). A priori one can only conclude that there are solutions to (1.1) that are close to a chaotic solution of the averaged system for a very long time (of $\mathcal{O}(1/\varepsilon^2)$). A chaotic solution is related to a full, bi-infinite sequence of N symbols by the horseshoe construction. The bounded validity of the averaging method only enables us to follow a chaotic solution over a bounded part of this sequence. To our knowledge, there are no general persistence results for chaotic solutions of an averaged system as chaotic solutions to the original system. This issue lies beyond the scope of this paper and will be considered in detail in [4].

Finally, we note that the approach developed in this paper, and in particular the construction and evaluation of the mixed Melnikov function, can also be used to study general nonlinear oscillators with similar 'almost resonant' quasi-periodic forcing terms (see also [15,26,27]). In the case of small amplitude oscillations, the only 'essential information' on the oscillator is T_2, the leading order quantity that describes the nonlinear character of the period of the periodic orbits of the nonlinear oscillator near the center point (2.8). This quantity can, of course, be determined for any nonlinear oscillator. Furthermore, the method can also be used to study more general resonances than just

the 1:1 case. In these cases, the averaged system will again have the character of a periodically forced integrable system. However, the integrable system for the higher resonances will have more than 'just' two homoclinic orbits [15]. For instance, there are two saddle points connected by four heteroclinic orbits in the 1:2 resonance. All orbits will 'break up' due to the periodic forcing term. The associated 'gaps' between the stable and unstable manifolds can again be measured by Melnikov functions, although one will need more than 'just' two 'classical' and one 'mixed' Melnikov function as we found in the $1:1$ case. As a consequence, there will also be more than the six different types of chaos/transversal intersections determined in this paper.

Acknowledgements

The authors thank Guido Terra for his careful reading of the manuscript and the (anonymous) referees for suggestions that helped to improve the presentation of the paper.

Appendix A. Explicit expressions for the unperturbed homoclinic orbits

By (3.8) and (3.9) we see that

$$S' = FY, \qquad 2FX = S^2 - 4\mathcal{H}^{\mathrm{hom}}, \tag{A.1}$$

on the homoclinic level set $\mathcal{H}(X, Y) = \mathcal{H}^{\mathrm{hom}}$ (recall that $S = (X^2 + Y^2) - 1$). Thus, X and Y can be removed from the differential equation for S

$$S' = \pm\sqrt{F^2(S+1) - \tfrac{1}{4}(S^2 - 4\mathcal{H}^{\mathrm{hom}})^2} = \pm\tfrac{1}{2}(S - S_{\mathrm{s}})\sqrt{(S - S_-)(S_+ - S)}, \tag{A.2}$$

where $S_+ > S_{\mathrm{s}} > S_-$ and

$$S_{\mathrm{s}} = X_{\mathrm{s}}^2 - 1 < 0, \quad S_\pm = -S_{\mathrm{s}} \pm \sqrt{\frac{-2F^2}{S_{\mathrm{s}}}}, \qquad \mathcal{H}^{\mathrm{hom}} = -\frac{3}{4}S_{\mathrm{s}}^2 - S_{\mathrm{s}}. \tag{A.3}$$

This equation can be brought into the form $\tilde{\mathrm{s}}' = \pm[$ the product of two linear terms in $\tilde{\mathrm{s}}]^{1/2}$ by introducing $\tilde{\mathrm{s}}(T) = \pm(S(T) - S_{\mathrm{s}})^{-1}$ (where the outer orbit corresponds with the $+$ and the inner with the $-$). The equation for $\tilde{\mathrm{s}}$ can be transformed into $\hat{\mathrm{s}}' = \mp\mu[\hat{\mathrm{s}}^2 + \hat{\mathrm{s}}_0^2]^{1/2}$ by setting $\tilde{\mathrm{s}}(T) = (1 + \hat{\mathrm{s}}(T)^2)\times$ a suitably chosen constant. This equation has two solutions of exponential growth (as $T \to \pm\infty$): $\hat{\mathrm{s}}(T) = \pm\hat{\mathrm{s}}_0 \sinh(\mu T)$. These solutions correspond to the homoclinic solutions of (A.2) as given in (3.11). It follows from a straightforward analysis that

$$A_{\mathrm{s}} = \frac{(S_{\mathrm{s}} - S_-)(S_+ - S_{\mathrm{s}})}{S_+ - S_-} > 0, \qquad a_{\mathrm{s}} = \frac{(S_+ + S_- - 2S_{\mathrm{s}})}{S_+ - S_-} \in (0, 1), \qquad \mu = \frac{1}{4}\sqrt{(S_{\mathrm{s}} - S_-)(S_+ - S_{\mathrm{s}})}. \tag{A.4}$$

Note that both orbits are biasymptotic to S_{s} and that $S_{\mathrm{out}}^{\mathrm{hom}}(0) = S_+$, $S_{\mathrm{in}}^{\mathrm{hom}}(0) = S_-$.

Appendix B. Computing $\mathcal{M}_{out}(T_0)$ and $\mathcal{M}_{in}(T_0)$

We (again) introduce $S_0(T) = (X_0(T)^2 + Y_0(T)^2) - 1$ and rewrite (3.14) by (3.12) and (A.1) as

$$\begin{aligned}\mathcal{M}_{\mathrm{out,in}}(T_0) = &-\frac{C}{8}\int_{-\infty}^{\infty}(3S_0^2 + 4S_0 + 4\mathcal{H}^{\mathrm{hom}})\,\mathrm{d}T + \frac{1}{4}\int_{-\infty}^{\infty}(S_0^2)'\sin(\Omega(T + T_0))\,\mathrm{d}T \\ &+\frac{1}{2}\int_{-\infty}^{\infty}S_0''\cos(\Omega(T + T_0))\,\mathrm{d}T.\end{aligned} \tag{B.1}$$

By expanding the $\cos(\Omega(T+T_0))$ and $\sin(\Omega(T+T_0))$ terms, and defining

$$\mathcal{J}_n(\Omega) = \int_{-\infty}^{\infty} (S_0(T) - S_s)^n \cos \Omega T \, \mathrm{d}T \tag{B.2}$$

for $n = 1, 2$, we can reduce (B.1) to

$$\mathcal{M}_{\mathrm{out,in}}(T_0) = -\frac{C}{8}[(4+6S_s)\mathcal{J}_1(0) + 3\mathcal{J}_2(0)] - \frac{\Omega}{4}[2(S_s+\Omega)\mathcal{J}_1(\Omega) + \mathcal{J}_2(\Omega)] \cos(\Omega T_0). \tag{B.3}$$

Note that all integrals involving $\sin(\Omega T)$ 'average out' since $S_0(T) - S_s$ is an even function of T (3.11). The $\mathcal{J}_n(\Omega)$ integrals can be evaluated by expressing them in terms of

$$\mathcal{I}(a,k) = \int_0^{\infty} \frac{\cos kx}{a + \cosh x} \, \mathrm{d}x = \frac{\pi}{\sin\phi} \frac{\sinh k\phi}{\sinh k\pi}, \tag{B.4}$$

where $a = \cos\phi \in [-1, 1]$ (this identity can be obtained by contour integration, see also [21]). At this stage we have to distinguish between the outer and the inner case. Based on (3.11) and (A.4) we define $\phi_{\mathrm{out,in}} = \phi_{\mathrm{out,in}}(F)$ as in (3.16). Thus, by (A.3) and (A.4)

$$S_s = -\frac{2}{3 + \tan^2\phi_{\mathrm{out,in}}}, \qquad \mu = \mp\frac{\tan\phi_{\mathrm{out,in}}}{3 + \tan^2\phi_{\mathrm{out,in}}}, \qquad A_s = 4\mu\sqrt{1 - \cos^2\phi_{\mathrm{out,in}}}. \tag{B.5}$$

Note that this also implies that

$$F = -\frac{4\cos^2\phi_{\mathrm{out,in}}}{(1 + 2\cos^2\phi_{\mathrm{out,in}})^{3/2}}. \tag{B.6}$$

Next, we introduce

$$k_s = k_s(\Omega, F) = \frac{\Omega}{2\mu}. \tag{B.7}$$

Like μ, k_s has the same value in the outer and the inner case (A.4). We thus find, for the outer case by (B.2), (B.4), (B.5) and (B.7)

$$\begin{aligned}
\mathcal{J}_1(\Omega) &= 4\sqrt{1-a_s^2}\,\mathcal{I}(a_s, k_s) = 4\pi \frac{\sinh k_s\phi_{\mathrm{out}}}{\sinh k_s\pi}, \\
\mathcal{J}_2(\Omega) &= -16\mu(1-a_s^2)\frac{\partial \mathcal{I}}{\partial a}(a_s, k_s) = 16\pi\mu \frac{\sinh k_s\phi_{\mathrm{out}}}{\sinh k_s\pi}\left(\frac{k_s}{\tanh k_s\phi_{\mathrm{out}}} - \frac{1}{\tan\phi_{\mathrm{out}}}\right).
\end{aligned} \tag{B.8}$$

Note that the limits $\Omega \to 0$ and $k_s \to 0$ are both well-defined. The computations for the inner case are in essence the same. The expressions given in (3.15) now follow from (B.3), (B.5) and (B.8).

References

[1] D. Beigie, A. Leonard, S. Wiggins, Chaotic transport in the homoclinic and heteroclinic tangle regions of quasiperiodically forced two-dimensional systems, Nonlinearity 4 (1991) 775–819.
[2] P. Chossat, Forced reflectional symmetry breaking of an O(2)-symmetric homoclinic cycle, Nonlinearity 6 (1993) 723–731.
[3] A. Defant, Physical Oceanography, Vol. II, Pergamon Press, Oxford, 1961.
[4] A. Doelman, G.M. Terra, The persistence of horseshoe maps in averaged systems, 2002, in preparation.
[5] W. Eckhaus, Asymptotic Analysis of Singular Perturbations, North-Holland, Amsterdam, 1979.
[6] T.W. Frison, H.D.I. Abarbanel, M.D. Earle, W.D. Scherer, Chaos and predictability in ocean water levels, J. Geophys. Res. 104 (4) (1999) 7935–7951.
[7] L.G. Golmen, J. Molvaer, J. Magnusson, Sea level oscillations with super-tidal frequencies in a coastal embayment of western Norway, Cont. Shelf Res. 14 (1994) 1439–1454.

[8] T. Green, Liquid oscillations in a basin with varying surface area, Phys. Fluids A 4 (1992) 630–632.
[9] J. Guckenheimer, P. Holmes, Nonlinear Oscillations, Dynamical Systems, and Bifurcations of Vector Fields, Applied Mathematical Science, Vol. 42, Springer, Berlin, 1983.
[10] K. Honda, T. Terada, Y. Yoshida, D. Isitani, Secondary undulations of oceanic tides, J. Coll. Sci. Imp. Univ. Tokyo 24 (1908).
[11] A.T. Ippen, Estuary and Coastline Hydrodynamics, McGraw-Hill, New York, 1966.
[12] C.K.R.T. Jones, T.J. Kaper, N. Kopell, Tracking invariant manifolds up to exponentially small errors, SIAM J. Math. Anal. 27 (1996) 558–577.
[13] C.K.R.T. Jones, N. Kopell, Tracking invariant manifolds with differential forms in singularly perturbed systems, J. Differential Equations 108 (1994) 64–88.
[14] O. Krümmel, Handbuch der Ozeanographie, Vol. 2, 2nd Edition, J. Engelhorn, 1911.
[15] A.Y. Levandovsky, Y.A. Tsarin, D.M. Vavriv, The interaction of resonances in a weakly nonlinear oscillator with a quasiperiodic excitation, Chaos 7 (2) (1997) 271–277.
[16] L.R.M. Maas, On the nonlinear Helmholtz response of almost-enclosed tidal basins with sloping bottoms, J. Fluid Mech. 349 (1997) 361–380.
[17] L.R.M. Maas, A. Doelman, Chaotic tides, J. Phys. Oceanogr. 32 (3) (2002) 870–890.
[18] A.P. Oost, Sedimentological implications of morphodynamic changes in the ebb-tidal delta, the inlet and the drainage basin of the Zoutkamperlaag tidal inlet (Dutch Wadden Sea), induced by a sudden decrease in the tidal prism, in: B.W. Flemming, A. Bartholomä (Eds.), Tidal Signatures in Modern and Ancient Sediments, Vol. 24, Spec. Pub. Int. Ass. Sediment., Blackwell, Oxford, 1995, pp. 101–119.
[19] G. Platzman, Two-dimensional free oscillations in natural basins, J. Phys. Oceanogr. 2 (1972) 117–138.
[20] V. Rom-Kedar, S. Wiggins, Transport in two-dimensional maps, Arch. Rational Mech. Anal. 109 (1990) 239–298.
[21] A.P. Prudnikov, Y.A. Bryckov, O.I. Marichev, Integrals and Series, Vol. I, Gordon and Breach, London, 1986.
[22] J.A. Sanders, F. Verhulst, Averaging Methods in Nonlinear Dynamical Systems, Applied Mathematical Sciences, Vol. 59, Springer, Berlin, 1985.
[23] G.M. Terra, L.R.M. Maas, A. Doelman, Weakly nonlinear dynamics of a co-oscillating tidal embayment, 2002, in preparation.
[24] G. Vittori, On the chaotic structure of tide elevation in the Lagoon of Venice, in: Proceedings of the 23rd International Conference on Coastal Engineering, 4–9 October 1992, Venice (Chapter 139).
[25] S. Wiggins, Introduction to Applied Nonlinear Dynamical Systems and Chaos, Texts in Applied Mathematics, Vol. 2, Springer, Berlin, 1990.
[26] K. Yagasaki, Second-order averaging and chaos in quasiperiodically forced weakly nonlinear oscillators, Physica D 44 (1990) 445–458.
[27] K. Yagasaki, Chaotic motions near homoclinic manifolds and resonant tori in quasiperiodic perturbations of planar Hamiltonian systems, Physica D 69 (1993) 232–269.
[28] J.T.F. Zimmerman, On the Lorentz linearization of a nonlinearly damped tidal Helmholtz oscillator, Proc. Kon. Ned. Akad. v. Wetensch. 95 (1992) 127–145.